Electrodeposited Sn-Cu-Ni alloys as lead-free solders on copper substrate using deep eutectic solvents

The influence of electrodeposition mode on the morphology, composition and corrosion behaviour

State, Sabrina Patricia; Costovici, Stefania; Mousavi, Mirsajjad; Garcia, Yaiza Gonzalez; Zanella, Caterina; Cojocaru, Anca; Anicai, Liana; Visan, Teodor; Enachescu, Marius

DOI
10.1016/j.surfcoat.2023.130324

Publication date
2024

Document Version
Final published version

Published in
Surface and Coatings Technology

Surface & Coatings Technology 477 (2024) 130324

Contents lists available at ScienceDirect

Surface & Coatings Technology

journal homepage: www.elsevier.com/locate/surfcoat

Electrodeposited Sn-Cu-Ni alloys as lead-free solders on copper substrate using deep eutectic solvents: The influence of electrodeposition mode on the morphology, composition and corrosion behaviour

Sabrina Patricia State (Rosoiu)[a,*], Stefania Costovici[a], Mirsajjad Mousavi[b], Yaiza Gonzalez Garcia[b], Caterina Zanella[c], Anca Cojocaru[a], Liana Anicai[a], Teodor Visan[a], Marius Enachescu[a]

[a] Center of Surface Science and Nanotechnology, University Politehnica of Bucharest, Splaiul Independentei 313, Bucharest 060042, Romania
[b] Department of Materials Science and Engineering, Delft University of Technology, Mekelweg 2, 2628 CD Delft, the Netherlands
[c] Department of Materials and Manufacturing, School of Engineering, Jönköping University, Gjuterigatan 5, 553 18 Jönköping, Sweden

ARTICLE INFO

Keywords:
Sn-Cu-Ni ternary alloy
Electrodeposition
Deep eutectic solvents
Corrosion behaviour
SVET

ABSTRACT

In this work we present the pulsed current (PC) electrodeposition of Sn-Cu-Ni alloy as lead-free solder candidate, from choline chloride – ethylene glycol eutectic mixtures (1:2 molar ratio) onto copper metallic substrates. Electrolytes containing Sn^{2+}, Cu^{2+} and Ni^{2+} salts in the selected deep eutectic solvent have been considered. The effect of the applied frequency of PC on the morphology, composition and melting point of the alloy is discussed and compared to the ones obtained using direct current (DC) plating mode. A refinement of the grain size and lower melting temperature of the alloy were noticed when pulsed current was applied.

A comparative analysis of the electrochemical corrosion behaviour at macro- and micro- scale has been performed in 0.5 M and 0.1 M NaCl solutions involving potentiodynamic polarization curves, electrochemical impedance spectroscopy (EIS) and scanning vibrating electrode (SVET) techniques. Furthermore, an analysis after 96 h of exposure to salt mist test simulating a corrosive attack in harsh environment is presented, too. The obtained results showed enhanced corrosion resistance of the ternary alloys electrodeposited under PC conditions (the best for 1.67 Hz frequency) as compared to those using DC. Additionally, Raman spectroscopy evidenced the presence of tin oxi/hydroxy chloride and tin oxides as surface corrosion products. A corrosion mechanism has been proposed.

1. Introduction

Under the current premises related to the restrictions on the use of hazardous materials in general and of the Pb containing ones in electronic industries in particular, the development of lead-free solders has gain considerable interest [1,2]. Therefore, various alloys containing mainly Sn and small amounts of different elements such as Cu, Ag, Zn, Ni, Sb, Bi, In, occasionally involving rare earth metals (*i.e.* Ce, La) have been proposed and investigated [3–5]. Sn-Ag-Cu and Sn-Cu alloys are usually considered as the most acceptable lead-free solders, exhibiting melting temperatures of 217–219 °C and 227 °C respectively [3,6]. A notable increase in interest was given to Sn-Cu alloys, as a more economical alternative, due to the elimination of silver content. It has been also shown that small additions of Ni to Sn-0.7Cu alloy could produce solders exhibiting crack-free surface, increased oxidation resistance, improved fluidity and lower copper dissolution rates [7–10]. Moreover, Sn-0.7Cu-0.05Ni solder was found to exhibit good corrosion resistance to long term exposure in aggressive environment [6,11,12]. The investigation of this type of lead-free solder alloy involving potentiodynamic polarization measurements and long-term immersion tests in 3.5 wt% NaCl solution showed higher corrosion rates as compared to Sn-Cu and Sn-Ag-Cu ones. Nevertheless, the longer exposure to the corrosive solution for, up to 30 days indicated that Sn-Cu-Ni alloy exhibited the slowest leaching rate of Sn in contrast to Sn-Cu and Sn-Ag-Cu systems.

Metallurgical methods are usually used to prepare Sn-Cu-Ni alloys as solders, based on the mixing of the pure elements in the right proportions, at high temperatures [13–15]. In the industry, there are several

* Corresponding author.
E-mail address: sabrina.rosoiu@upb.ro (S.P. State).

https://doi.org/10.1016/j.surfcoat.2023.130324
Received 31 August 2023; Received in revised form 6 December 2023; Accepted 16 December 2023
Available online 21 December 2023

Table 1
Electrolyte composition for Sn-Cu-Ni alloy electrodeposition.

DES type	Electrolyte composition
Choline chloride:ethylene glycol (1:2 molar ratio)-ILEG	500 mM $SnCl_2{\cdot}2H_2O$ 0.055 mM $NiCl_2{\cdot}6H_2O$ 0.345 mM $CuCl_2{\cdot}2H_2O$

solder deposition techniques being utilized, including screen printing, robotic ball placement, evaporation and electrodeposition [16,17]. Electrodeposition represents a simple and cost-effective procedure to synthesize lead-free solder alloys showing good end properties, also being easily scaled up to industrial level production [16,18]. A promising alternative to the traditional involvement of aqueous electrolytes during alloy electrochemical deposition is represented by the use of deep eutectic solvents (DESs). These are a novel category of ionic liquids (ILs) analogues, as they exhibit numerous characteristics and properties similar to those found in conventional ILs [19]. Usually, DESs are obtained by combining a hydrogen bond acceptor, commonly a quaternary ammonium salts with either a hydrogen bond donor or a metal salt [20–22]. They exhibit remarkable stability concerning air and moisture, are cost effective and represent a more environmentally friendly alternative to traditional water-based electrolytes.

Rao et al. [23] electrochemically prepared porous Sn-Ni-Cu alloy on Ni foam under potentiostatic conditions at −0.4 V *vs.* Ag ref. from a DES electrolyte based on choline chloride: ethylene glycol (1:2 molar ratio), using nickel matte as the primary raw material, resulting in the final electrolyte containing 0.06 M Ni^{2+}, 0.03 M Cu^{+} and 0.12 M Sn^{2+}. It has been concluded that the cathodic potential significantly influenced the microstructure of the alloy film. Very recently, the synthesis of Sn-Cu-Ni alloys as lead-free solders from DES based electrolytes, using Cu as metallic substrate has been reported in [24]. The Sn-0.65Cu-0.06Ni stoichiometry, which closely aligns with industrial recommendations for electronics, has been obtained through a fine adjustment of the concentration of the metallic salts in the solutions and the applied current density. The assessment of the solder joint performance revealed satisfactory solderability properties and good adhesion of the deposit to the substrate without any fracture.

The metals and alloys electrodeposited from DES solutions, usually involve the use of direct current (DC) [20]. Pulse current (PC) plating refers to the electrochemical deposition method that involves the application of periodic current [25,26], represents a more efficient and feasible approach to enhance the quality of metallic coatings. Usually, PC electrodeposition method present advantageous effects on the microstructure, morphology, ductility, hardness and surface roughness of coatings, while simultaneously enabling the use of higher applied current density values. Moreover, the electrodeposition involving pulse current can modulate the composition of the deposits [27]. A large range of electroplating parameters such as peak current density, pulse frequency, duty cycle, and on/off time can be adjusted in PC mode.

There has been limited reporting on the utilization of PC electrodeposition in DES based electrolytes. Rosoiu et al. [28] presented the use of PC method during electrodeposition of Ni-Sn alloy from choline chloride: ethylene glycol eutectic mixture. A decrease of the crystallite size and an improvement of the mechanical properties were noticed on applying PC. Xing et al. [29] conducted a study on the PC electrodeposition of Cu involving choline chloride: ethylene glycol (1:2 molar ratio) electrolyte and showed notable enhancement in the current efficiency. Anicai et al. [30] found that employing PC plating during Sn-In alloy electrodeposition from choline chloride-ethylene glycol eutectic mixtures yielded to a deposit that is more uniform and compact compared to the ones obtained under DC conditions. Furthermore, they observed a slight reduction in particle size, down to 1.0–1.2 μm. The PC procedure enabled the application of higher current densities, leading to a slight increase in the In content within the alloy deposit. Pallaro et al. [31] applied PC to electrodeposit Sn-Cu alloy involving an ethylene glycol solution. SEM investigations revealed that the use of PC allowed a better homogeneity of the coating and a decrease of the surface defects.

The corrosion performance of solder alloys is important during long-term service or when the solder joints are directly exposed to aggressive industrial environment [32,33]. Relatively few studies have been reported on the corrosion behaviour of lead-free solder alloys [33], mostly centered on the binary Sn-Zn, Sn-Cu, Sn-Ag, Sn-Bi, and the ternary Sn–Ag–Cu systems. Only Guerrero et al. [12] discussed the anticorrosive properties of the ternary Sn-0.7Cu-0.05Ni alloys and joints (with copper substrate) in 3.5 wt% NaCl solution. They found that the leaching rate of Sn in Sn-0.7Cu-0.05Ni alloys after longer exposure to the aggressive environment during 30 days was the lowest, as compared to Sn-Cu and Sn-Ag-Cu solders. The galvanic coupling between Sn, as the main constituent of the solder, and Cu from the substrate, accelerates the corrosion process and leads to higher Sn leaching rate in the joint solder as compared to the bare alloy. According to the performed EDS and XRD investigations, the main constituents of the corrosion products are tin oxides, accompanied by small amounts of chlorides. The reported corrosion investigations of the ternary Sn-Cu-Ni alloy system were performed at macro-scale, mostly involving potentiodynamic polarization and electrochemical impedance spectroscopy, as traditional electrochemical techniques [12,24].

Scanning vibrating electrode technique (SVET) is an adequate technique to obtain information on corrosion processes at microscopic level. With its distinctive capability to visualize the local current density of an active specimen in electrolyte, this method offers a highly sensitive approach to monitor dynamic processes, such as corrosion, as it occur. During SVET experiments, a vibrating microelectrode scans the surface of the sample while it is immersed in the corrosive environment and detects *in situ* the anodic and cathodic regions related to the corrosion processes [34,35]. Isaacs used the scanning vibrating electrode technique to investigate the galvanic corrosion of Sb-Sn and Sn-Pb alloys after soldering to copper using a dilute chloride/sulphate solution in air [36]. It has been shown that Sb-Sn alloy soldered to copper was susceptible to localized corrosion, while Sn-Pb exhibited a passive behaviour.

In previous work [24], the authors investigated the synthesis of Sn-Cu-Ni ternary alloy under DC mode from a DES based-electrolyte consisting in the eutectic mixture of choline-chloride with ethylene glycol (1:2 molar ratio), comprising specific ratio of the metallic salts to achieve the industrial stoichiometry (Sn99.29-Cu0.65-Ni0.06) for lead-free soldering alloy. The conducted research indicated that the morphology of the alloy shows individual particles distributed over the entire copper substrate.

Considering all mentioned above, the present work focuses on the Sn-Cu-Ni alloy electrodeposition from choline chloride – ethylene glycol eutectic mixtures onto copper metallic substrates under pulse plating regime, at a fixed average current density and duty cycle, while the pulse frequency was varied. Particular emphasis was given to the influence of the applied frequency on the morphology, composition and melting point of the alloy deposit. Furthermore, a comparative analysis of the electrochemical corrosion behaviour of the ternary alloy obtained by electrodeposition under direct (DC) and pulse (PC) plating conditions is performed at macro- and micro-scale, involving potentiodynamic polarization curves, electrochemical impedance spectroscopy (EIS) and scanning vibrating electrode (SVET) techniques in 0.5 M and 0.1 M NaCl solutions In addition, salt mist tests were performed to mimic a corrosive attack in aggressive environment. Raman spectroscopy was employed to gain additional insights about the corrosion products and a proposed corrosion mechanism is discussed. To the best of our knowledge, such studies on the ternary Sn-Cu-Ni alloy, especially from DES based electrolytes, have not been described in literature so far.

Table 2
Electrodeposition parameters.

System type	Operating parameters			
	On- and off-time duration of the pulse	Frequency (Hz)	Duty cycle (%)	Current density (mA/cm^2)
Sn-Cu-Ni-DC	–	–	–	8
Sn-Cu-Ni-P1	$T_{ON} = 0.01$ s $T_{OFF} = 0.05$ s	16.67	16.7	8
Sn-Cu-Ni-P2	$T_{ON} = 0.10$ s $T_{OFF} = 0.5$ s	1.67	16.7	8
Sn-Cu-Ni-P3	$T_{ON} = 1$ s $T_{OFF} = 5$ s	0.167	16.7	8
Sn-Cu-Ni-P4	$T_{ON} = 10$ s $T_{OFF} = 50$ s	0.0167	16.7	8

2. Materials and methods

2.1. Electrolyte synthesis and electrodeposition of Sn-Cu-Ni ternary alloy

Choline chloride was mixed with ethylene glycol in a 1:2 molar ratio (denoted as ILEG) and heated at 80–90 °C until a transparent liquid was produced. Furthermore, tin, nickel and copper salts, corresponding to the target alloy, were added into the electrolyte under continuous stirring and heating at 90 °C. The final composition of the electrolyte, as it has been previously optimized [24], is presented in Table 1. The prepared electrolyte has been stored in airtight glass recipients to minimize its interaction with air and atmospheric moisture.

All the involved chemicals, respectively choline chloride (ChCl) (Merck, >98 %), ethylene glycol (Silal Trading Bucharest, 99 %), tin chloride ($SnCl_2{\cdot}2H_2O$, Acros Organics, >97 %), copper chloride

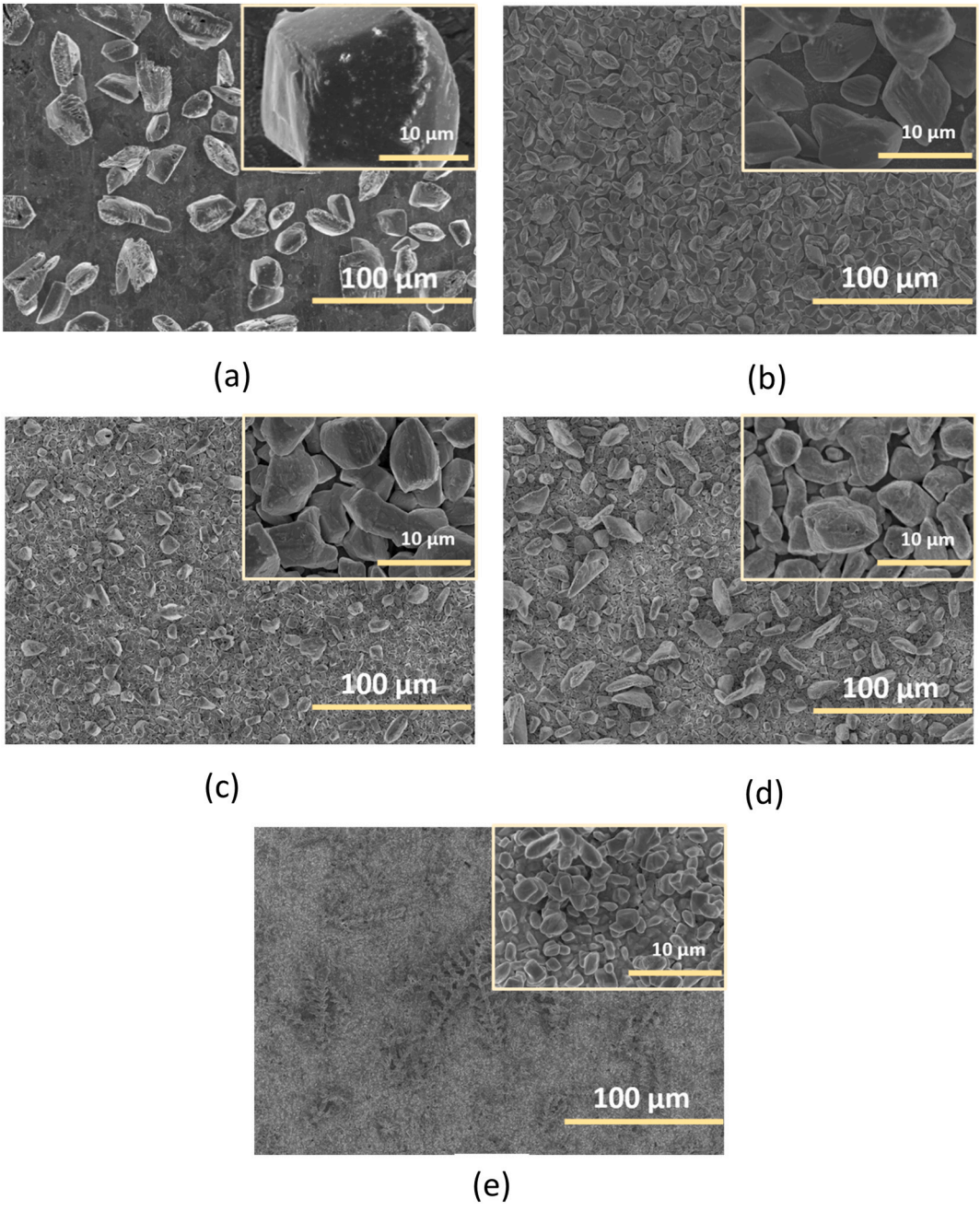

Fig. 1. SEM images of Sn-Cu-Ni ternary alloys synthetized from ILEG based electrolyte: (a) Sn-Cu-Ni-DC; (b) Sn-Cu-Ni-P1; (c) Sn-Cu-Ni-P2; (d) Sn-Cu-Ni-P3 and (e) Sn-Cu-Ni-P4 (the applied DC and PC parameters as detailed in Table 2).

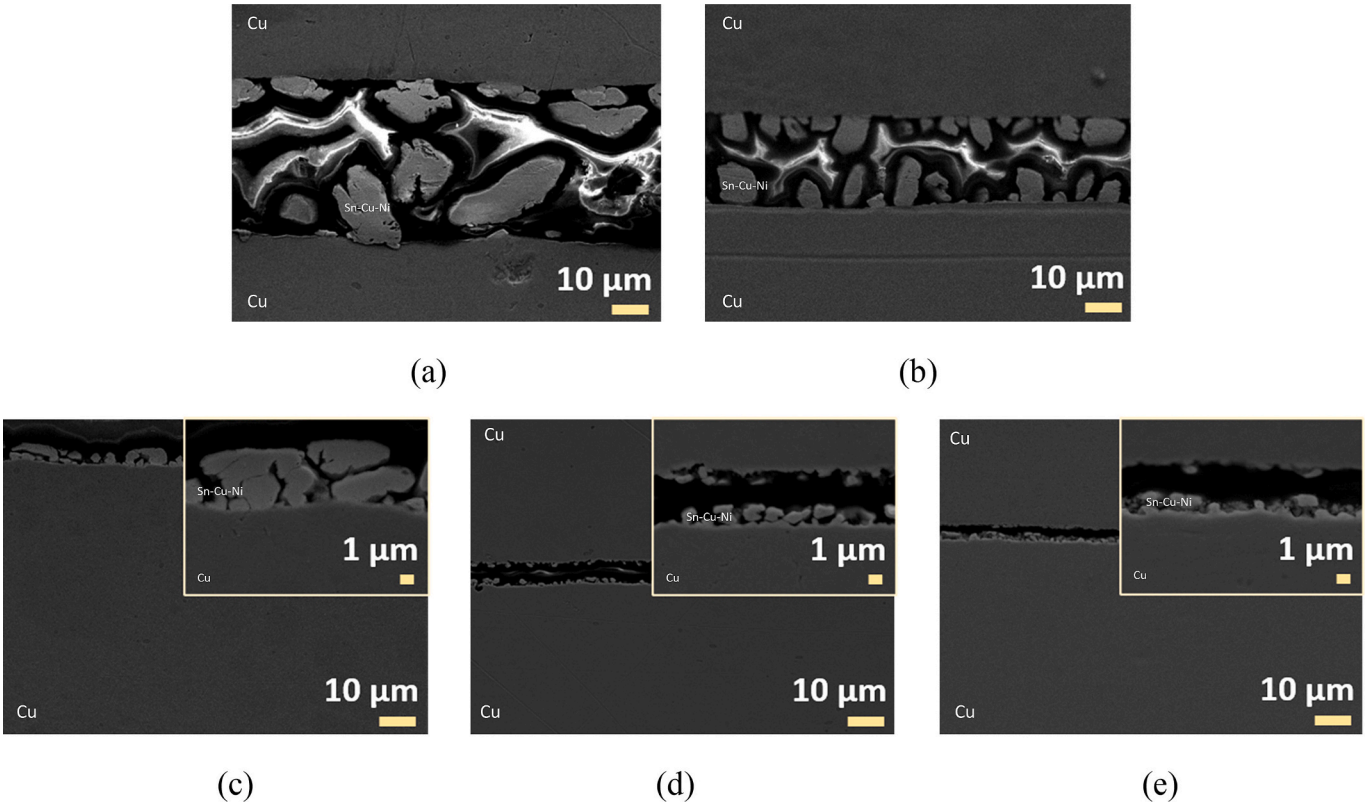

Fig. 2. Cross section SEM images of Sn-Cu-Ni ternary alloys synthetized from ILEG based electrolyte: (a) Sn-Cu-Ni-DC; (b) Sn-Cu-Ni-P1; (c) Sn-Cu-Ni-P2; (d) Sn-Cu-Ni-P3 and (e) Sn-Cu-Ni-P4 (the applied DC and PC parameters as detailed in Table 2).

Table 3
Melting temperature values and composition of the Sn-Cu-Ni alloys synthetized in DC and PC plating mode.

Sn-Cu-Ni alloy system	T_{onset} (°C)	Composition (wt.%)		
		Sn	Cu	Ni
Sn-Cu-Ni-DC	229.4	99.29 ± 0.25	0.65 ± 0.10	0.06 ± 0.02
Sn-Cu-Ni-P1	230.2	99.34 ± 0.36	0.44 ± 0.16	0.22 ± 0.07
Sn-Cu-Ni-P2	228.6	98.66 ± 0.81	0.44 ± 0.13	0.90 ± 0.20
Sn-Cu-Ni-P3	226.9	98.30 ± 1.00	0.68 ± 0.15	1.02 ± 0.56
Sn-Cu-Ni-P4	227.0	97.69 ± 0.77	1.40 ± 0.27	0.91 ± 0.36

($CuCl_2{\cdot}2H_2O$, VWR Chemicals, 99 %) and nickel chloride ($NiCl_2{\cdot}6H_2O$, Lach-Ner Ltd, 99 %) were used as received. The water content for the prepared electrolyte was determined by Karl-Fischer titration (Titro-Line1 7500 KF trace titrator) and values in the range 0.1–0.5 % have been measured.

The ternary alloy has been electrodeposited using a two- electrode cell configuration and a pulse reverse power supply pe86CB3HE (Plating Electronic GmbH). The anode was a graphite plate (S = 10 cm^2). The alloy has been electrodeposited on copper sheets as cathodes of 0.2 mm thickness and 7.5 cm^2 working area. Prior to the plating, the specimens were subjected to a surface pre-treatment consisting in acetone cleaning, followed by chemical microetching using H_2SO_4:H_2O_2:H_2O (5/10/85 vol%) solution for 30 s at RT, then rinsed with deionized water and air dried. The roughness of the Cu substrate after the surface pre-treatment was 177.8 nm Sn-Cu-Ni alloy deposits were obtained involving both direct current (DC) and pulse current (PC) conditions. During PC plating the used square pulsed parameters are defined according to the following equations:

$$J_{av} = \frac{i_p T_{on}}{T_{on} + T_{off}} \quad (1)$$

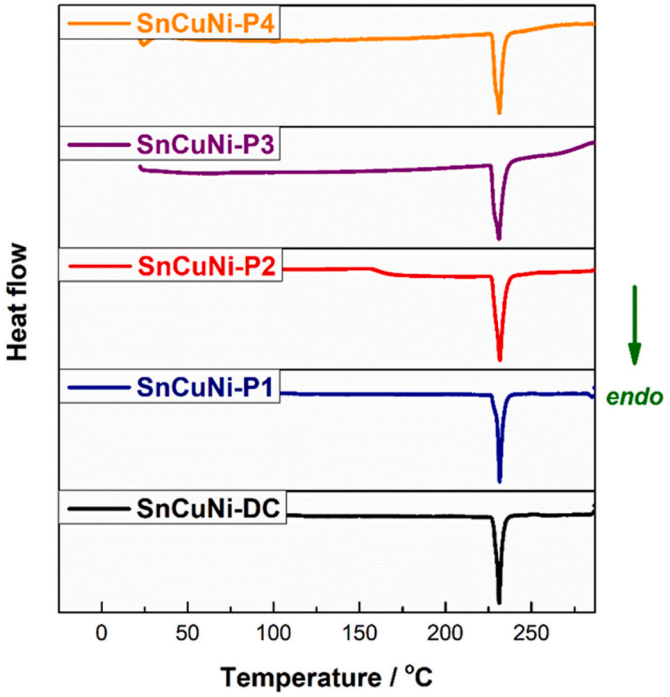

Fig. 3. Differential scanning calorimetry (DSC) analysis of the Sn-Ni-Cu ternary alloys synthetized under DC (Sn-Cu-Ni-DC) and PC (Sn-Cu-Ni-P1, Sn-Cu-Ni-P2, Sn-Cu-Ni-P3 and Sn-Cu-Ni-P4) plating modes.

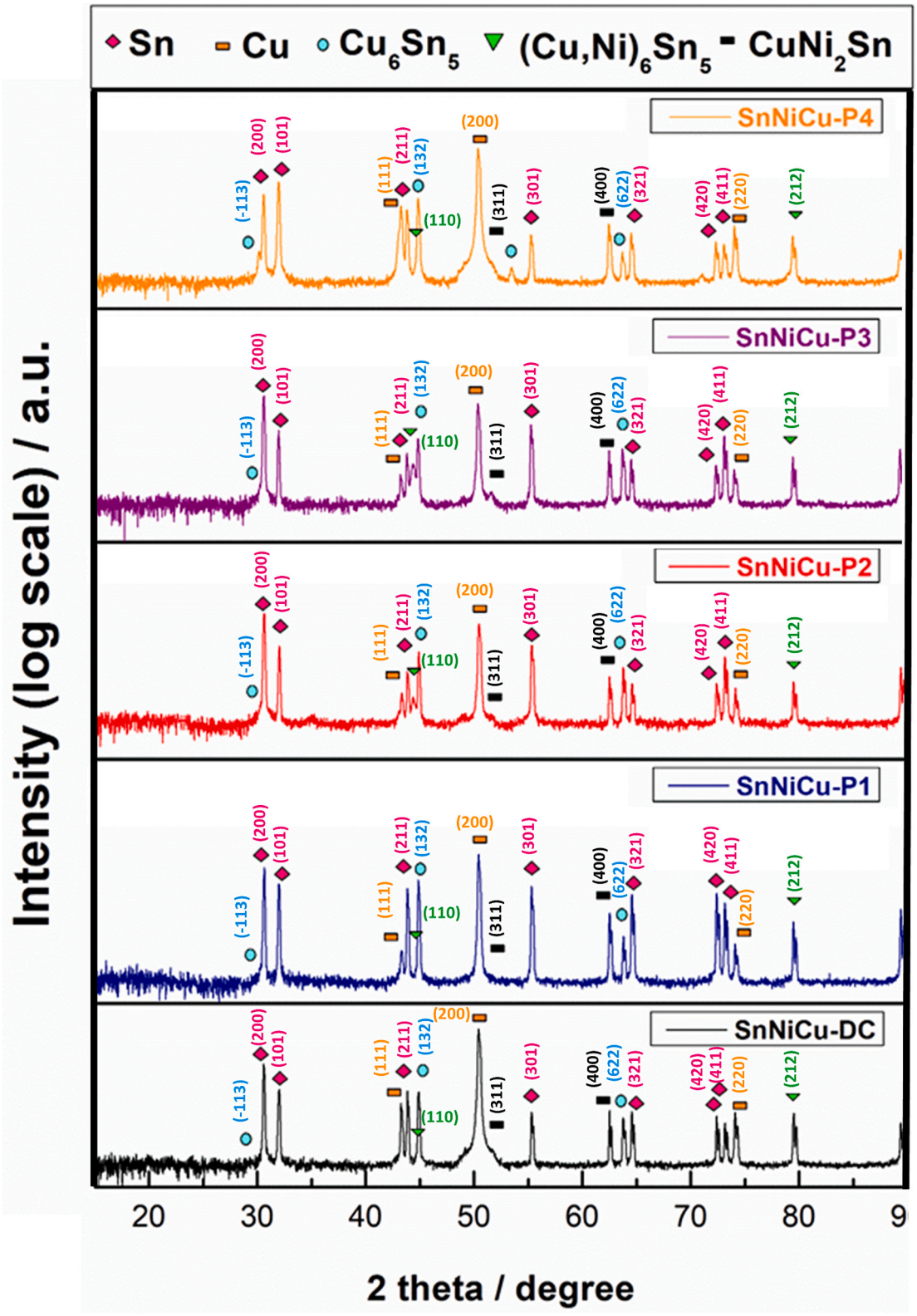

Fig. 4. X-ray diffractograms of Sn-Ni-Cu ternary alloys synthetized under DC (Sn-Cu-Ni-DC) and various PC (Sn-Cu-Ni-P1, Sn-Cu-Ni-P2, Sn-Cu-Ni-P3, and Sn-Cu-Ni-P4) plating modes.

$$f = \frac{1}{T_{on} + T_{off}} \quad (2)$$

$$\theta = \frac{T_{on}}{T_{on} + T_{off}} \cdot 100 \quad (3)$$

where J_{av} is the average current density, i_p is the peak current density, T_{on} and T_{off} are the on- and off- current time periods, and f and θ are the pulse frequency and duty cycle, respectively. All the deposits were obtained at 8 mA/cm^2 (constant current density in DC and average current density in PC). For PC electrodeposition conditions, the duty cycle was

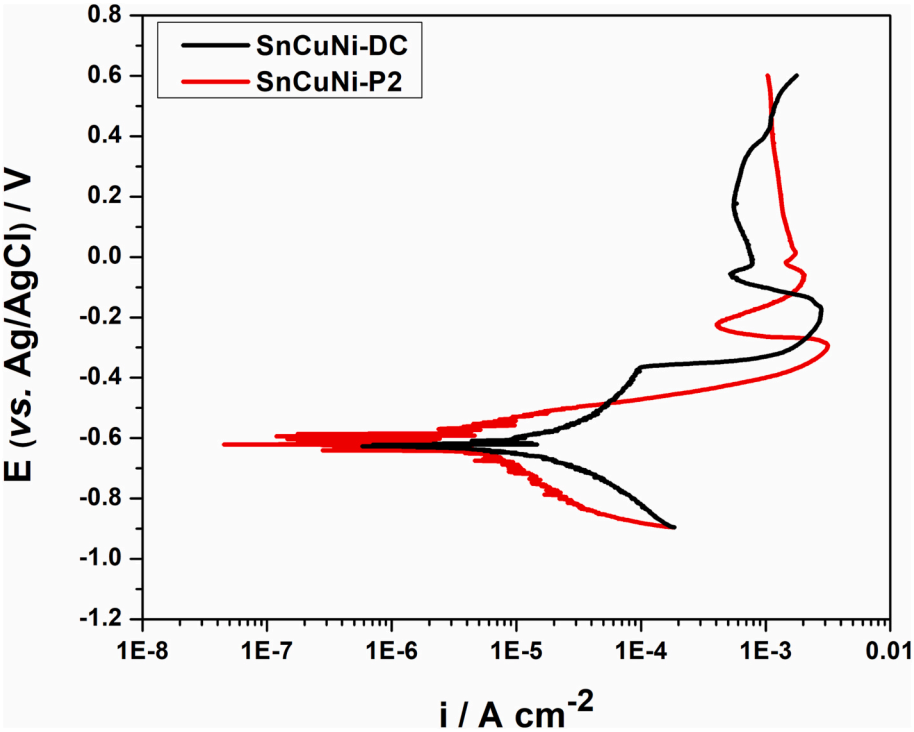

Fig. 5. Polarization curves for Sn-Cu-Ni ternary alloys synthesized under DC and PC plating modes in 0.5 M NaCl (25 °C, 1 mV s^{-1}), represented in semilogarithmic coordinates.

fixed at 16.7 %, while the frequency was varied: 16.67 Hz, 1.67 Hz, 0.167 Hz and 0.0167 Hz. The electrodeposition was performed during 30 min at 60 °C under stirring. The operating parameters are detailed in Table 2. After electrochemical process, the alloys underwent cleaning using heated deionized water, followed by. acetone, and were subsequently dried using air.

In order to determine the melting point of the ternary alloys, the electrodeposition process under DC and PC conditions for some samples was performed for 90 min on a non-adherent substrate, titanium (Ti) metallic substrate (S = 7.5 cm^2). The alloy was further detached from the Ti substrate and the resulted deposits were cleaned with hot deionized water, acetone and air-dried. Prior to the electrodeposition, the Ti cathode was subjected to mechanical grinding and chemical pickling in 1:1 HNO_3: H_2O solution at 25 °C for 30 s, then rinsed with distilled water and air dried. The roughness of the Ti substrate prior to electrodeposition was 431.0 nm.

2.2. Characterization of Sn-Cu-Ni ternary alloy deposits

Scanning Electron Microscopy (SEM) (Ultra-high Hitachi SU 8230 microscope and JEOL JSM-7001F FE-SEM microscope) associated with the Energy Dispersive X-ray spectroscopy (EDX) (Oxford Instruments) were employed for morphological and elemental composition analysis. The Image J software was involved to analyse the SEM images. X-ray diffraction (XRD) (High Resolution SmartLab X-ray diffractometer Rigaku, 9 kW) having CuK_α radiation (λ = 0.15406 nm), working in the range from 5 to 90 degree was used to obtained more information about the structure of the alloys. The thermal properties of the ternary alloys were studied by differential scanning calorimetry (DSC) using Shimadzu DSC 50 calorimeter under argon atmosphere applying a heating rate of 10 °C/min from RT to 300 °C. Raman studies were performed involving the LabRam HR800 Horiba equipment using He-Ne laser, 532.18 nm wavelength and 0.85 mW. All the data were processed using Origin 8.5 software.

In addition, atomic absorption spectroscopy – AAS (ContrAA 700 for flame technique – Analytik Jena) was used to get more information about the alloy composition. The AAS quantitative analysis was performed on 0.1–0.2 g of electrodeposited alloys.

2.3. Electrochemical corrosion studies

The anticorrosive properties of as electrodeposited Sn-Cu-Ni alloy coated copper substrate were assessed by potentiodynamic polarization measurements, having the sweep rate fixed at 1 mV s^{-1} and the electrochemical impedance spectra (EIS) were recorded from OCP in 0.5 M NaCl aqueous solution at RT, with a PARSTAT 4000 potentiostat equipped with VersaStudio software. For EIS, the following parameters were set: 10 mV ac voltage and 100 kHz–100 mHz frequency range. The recorded data were analysed using ZView 2.4 software (Scribner Association Inc., Derek Johnson). The surface of working electrode was 0.63 cm^2, Pt plate was used as the counter electrode, while Ag/AgCl was the reference electrode.

The local SVET experiments were carried out in 0.1 M NaCl solution at RT using Applicable Electronics LLC equipped with ASET software. For SVET analysis low concentration of NaCl solution is used to minimize the interference of the solution conductivity in the recorded signal. The samples were sealed with non-conductive, corrosive-resistant polymer and only a surface area of ~3 mm^2 (DC)/0.5 mm^2 (PC) was left uncovered. The investigated specimens have been exposed for 168 h (one week) to the aggressive electrolyte and the SVET measurements were carried out initially and after various immersion periods of 24 and 168 h. Platinum iridium alloy (Pt-Ir) needles were used as vibrating tips on which a Pt black sphere of ~30 μm was deposited. The tips were calibrated prior to measurements and during the SVET analysis the probe was set at a distance of 100 μm above the surface of the samples. The data were analysed with Quikgrid software. In addition, the resistance to harsh corrosive environment has been assessed by salt-spray tests performed according to ASTM B117-2019 [37] and ISO 9227-2017 standards [38]. Printed circuit boards (PCBs) specimens whose pads were coated with Sn-Cu-Ni alloys involving DC and PC plating conditions were exposed for a period of 96 h at 35 °C to neutral salt fog (Erichsen Model 606 equipment) at a pH of 6.5–7.2. The specimens have

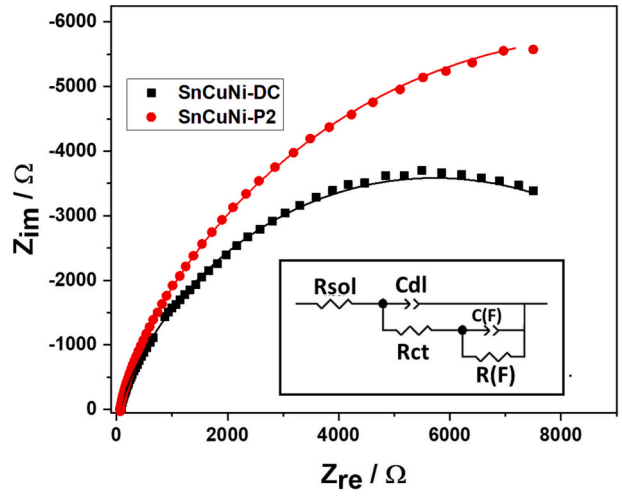

(a)

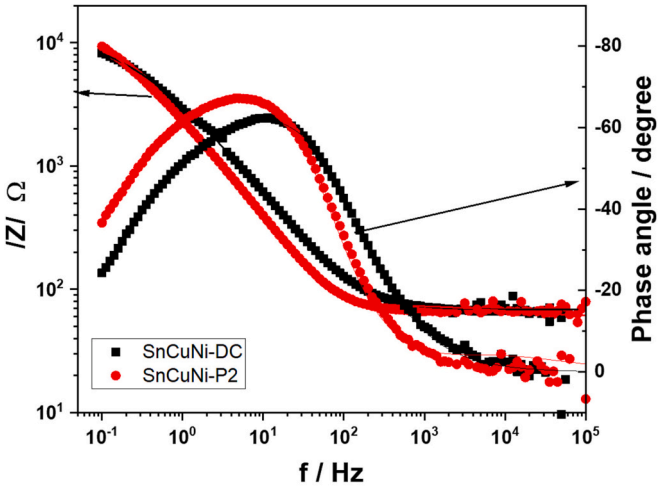

(b)

Fig. 6. Nyquist (a) and Bode (b) plots for Sn-Cu-Ni ternary alloys synthetized under DC and PC plating modes in 0.5 M NaCl at open-circuit potential (the equivalent circuit for the fitting analysis is represented in the inset of figure (a)).

Table 4
EIS fitting parameters for Sn-Cu-Ni ternary alloys.

Parameter	System	
	Sn-Cu-Ni-DC	Sn-Cu-Ni-P2
R_{sol}/Ω cm^2	37.4	34.6
R_{CT}/Ω cm^2	8.1	11.3
$C_{dl\ (CPE\ 1)}$/Ω^{-1}·s^n cm^{-2}	92.8	129.8
$n_{(CPE\ 1)}$	0.6	0.62
R_F/Ω cm^2	7541	12,238
$C_{F\ (CPE\ 2)}$/μF cm^{-2}	37.5	43.3
$n_{(CPE\ 2)}$	0.90	0.99
χ^2	2.71 × 10^{-3}	1.80 × 10^{-3}

been subjected to intermediary examinations after 24, 48, 72 and 96 conditioning hours using an optical microscope at 5× magnification and SEM. The samples were exposed to the mentioned corrosion tests as resulted after electrodeposition. For each experiment, at least three specimens were analysed.

The investigation of the anticorrosive properties of the Sn-Cu-Ni alloy coated copper substrate was performed considering the geometrical area. The influence of the sample's roughness on the exposed surface to NaCl solutions has not been assessed.

3. Results and discussion

3.1. Electrodeposition of Sn-Cu-Ni ternary alloys under DC and PC conditions

Previous studies have demonstrated [24] that is feasible to deposit adherent, uniform and bright Sn-Cu-Ni alloy coatings onto Cu substrate under DC conditions at an optimum applied current density of 8 mA/cm^2 from choline chloride based deep eutectic solvents. The same value has been employed further in this study as average current density (i_{av}) during PC plating, performed at a fixed duty cycle of 16.7 %. Since the current density was intended to be kept constant for DC and PC electrodeposition modes, the peak current density for pulse plating was set much higher, i_p = 48 mA/cm^2. This is one of the advantages of pulse current plating, since very high instantaneous current densities can be applied [39].

The SEM micrographs comparatively illustrating the surface morphology of the electrodeposited Sn-Cu-Ni alloy coatings under DC and under PC at various frequencies, as well as their cross section are presented in Figs. 1 and 2, respectively. The use of DC (see Fig. 1a) produced alloy deposits exhibiting a cubic morphology with large irregular grains. In addition, the presence of some gaps between the grains could be noticed from Fig. 2a, suggesting the formation of a less compact deposit when DC conditions were applied.

To enhance the quality of the electrodeposited Sn-Cu-Ni alloy coatings in terms of morphology and compactness, the use of PC plating mode has been explored. It is worth mentioning here that DESs exhibit different characteristics as compared to aqueous electrolytes, including electrical conductivities, their double-layer structure, mass transport properties and electrochemical kinetics. Therefore, the adequate pulse conditions to perform electrodeposition are dissimilar to those applied for aqueous systems [40,41]. It has been found out that high frequencies of pulses (in the order of hundreds hertz) are not appropriate when DESs or traditional ionic liquids are involved [31,42,43]. As shown in Figs. 1b–e and 2b–e, the variation of the applied frequency determines a significant change of the alloy deposit morphology. More compact coatings could be observed, as the applied frequency is lower. In addition, the cross-section SEM images show the presence of a continuous layer below the grains when PC conditions are applied.

The mean grain size of the alloy deposits was determined with the Image J software. Thus, the use of DC conditions led to the formation of coatings exhibiting granular particles of 16.7 ± 4.1 μm, larger than those calculated when PC was applied. Therefore, values of 7.4 ± 2.4, 4.3 ± 1.7, 3.1 ± 1.2 and 1.4 ± 0.5 μm were calculated for Sn-Cu-Ni-P1, Sn-Cu-Ni-P2, Sn-Cu-Ni-P3 and Sn-Cu-Ni-P4, corresponding to applied frequencies of 16.67 Hz, 1.67 Hz, 0.167 Hz and 0.0167 Hz, respectively. A decrease of the grain size could be noticed as the pulse frequency is lower. This behaviour is different from what have been reported for Sn electrodeposition in water-based electrolytes where a decrease of the grain size was observed while increasing the applied frequency [44]. Considering the DES based electrolyte's relatively high viscosity and the size of the metal cations, longer duration may be necessary for diffusion from the bulk solution to the cathode surface. Therefore, during T_{ON} time, the concentration of the metallic ions is diminished while during the T_{OFF} period their amount at the cathode surface is partially recovered. In other words, the system is allowed to relax before new grains to

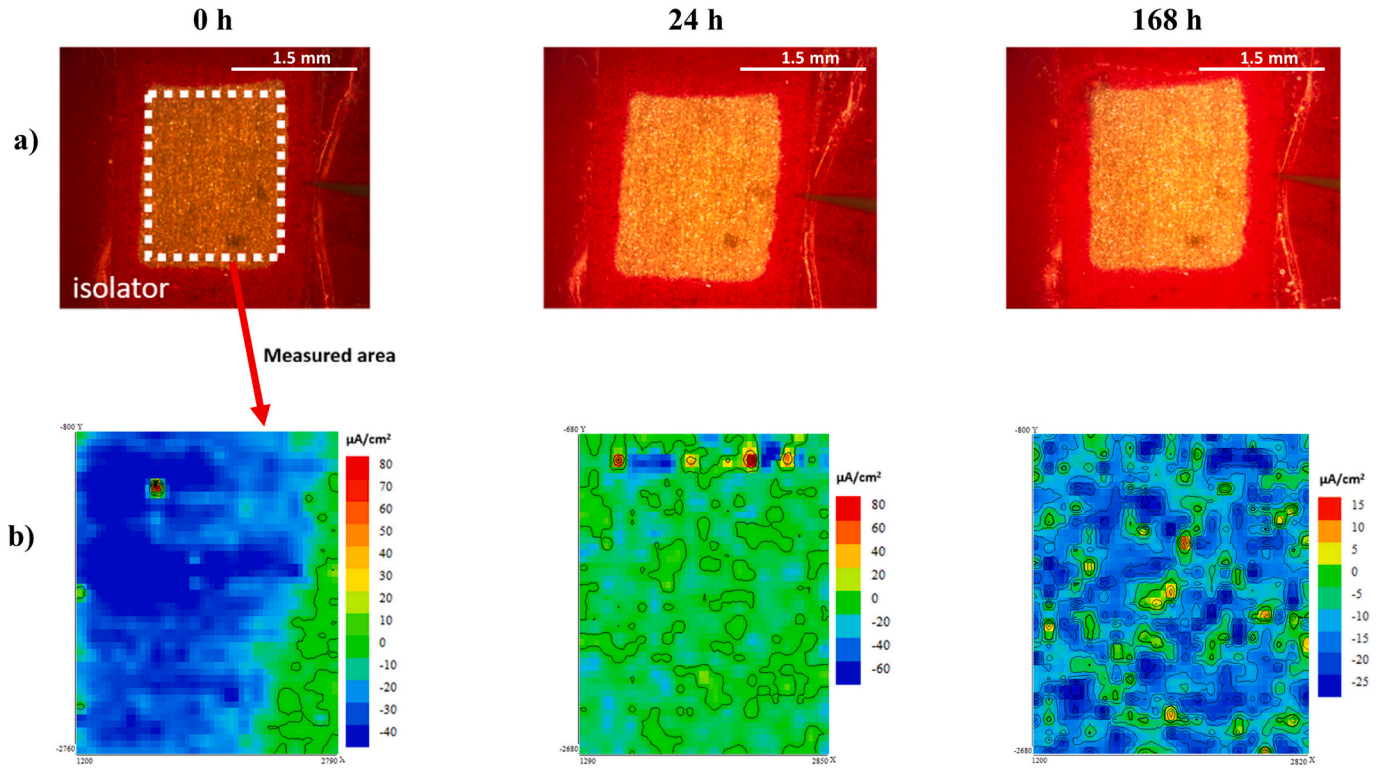

Fig. 7. SVET measurements of Sn-Cu-Ni-DC specimen after various immersion periods in 0.1 M NaCl: (a) optical images prior SVET measurements; (b) maps of the current density distribution of the surface.

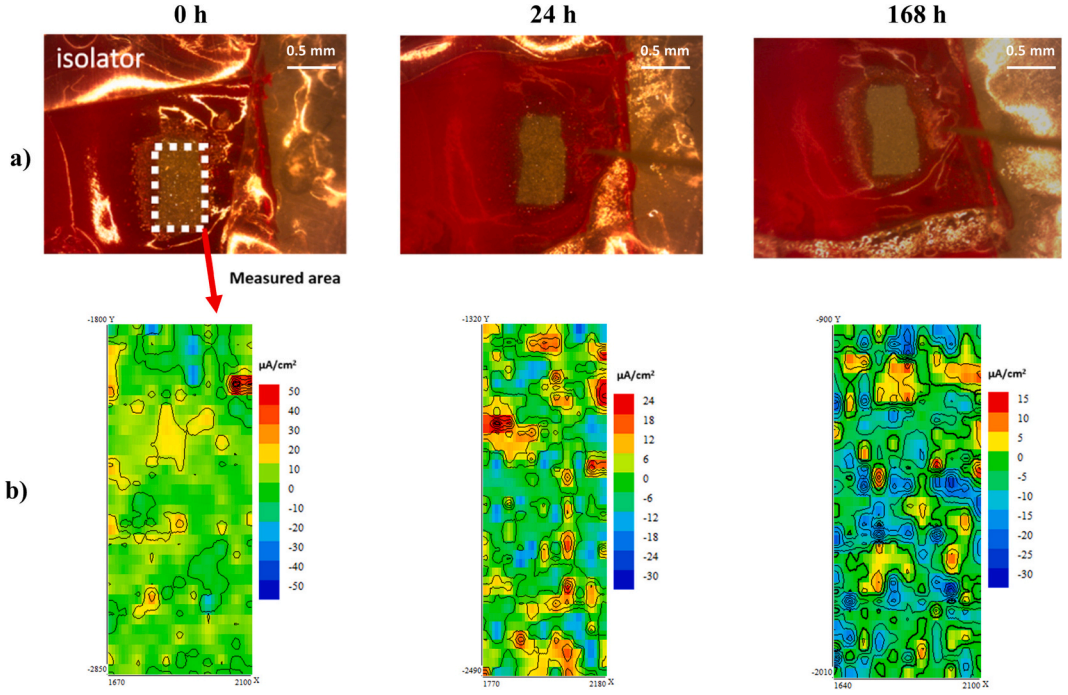

Fig. 8. SVET measurements of Sn-Cu-Ni-P2 specimen after various immersion periods in 0.1 M NaCl: (a) optical images prior SVET measurements; (b) maps of the current density distribution of the surface.

be formed or continue to grow, a process that has a positive effect on the final quality of the deposit [31,42].

The current efficiency during Sn-Cu-Ni alloy electrodeposition under DC and PC conditions has been also analysed. When DC plating has been applied, an efficiency value of 51 ± 1.3 % has been determined, while a gradual decrease was observed under PC deposition, from 34 ± 0.5 % to 31 ± 0.9 %, 26 ± 1 % and 17 ± 1.5 % as the applied frequency has been reduced from 16.67 Hz to 1.67 Hz, 0.167 Hz and 0.0167 Hz, respectively. Even the current density in DC has the same value as average current density in PC plating, it should bear in mind that under PC the

Table 5
The ionic currents resulting from the cathodic and anodic half-reactions for Sn-Cu-Ni-DC system.

Immersion period (h)	Integrated anodic current (μA)	Integrated cathodic current (μA)
Initial	2.27×10^{-2}	-8.55×10^{-1}
24	1.10×10^{-1}	-3.00×10^{-1}
168	3.28×10^{-2}	-4.03×10^{-1}

Table 6
The ionic currents resulting from the cathodic and anodic half-reactions for Sn-Cu-Ni-P2 system.

Immersion period (h)	Integrated anodic current (μA)	Integrated cathodic current (μA)
Initial	4.47×10^{-2}	-1.16×10^{-2}
24	3.26×10^{-2}	-2.40×10^{-2}
168	1.58×10^{-2}	-3.60×10^{-2}

peak current density present a significant increase, by six times, compared the value for DC plating so that side reactions including hydrogen evolution could be more significant, affecting the overall process [45]. In addition, within the PC conditions, the current efficiency tends to decrease as the applied frequency is lower. This phenomenon could be related to the longer T_{ON} periods when the high current is applied, leading to a faster depletion of the ions near the cathode. The same behaviour has been reported by Green et al. [41] and by Rosoiu et al. [28] during PC plating of Cu and Ni-Sn alloy respectively, involving choline chloride-ethylene glycol eutectic mixture, when a partial dissolution of the metals during the "off time" has been also considered.

The influence of DC and PC method on the composition and on the melting point of the obtained Sn-Cu-Ni alloy deposits has been investigated by EDX analysis and DSC, respectively. To mitigate the influence of the substrate on the quantity of Cu within the deposit, the electrodeposition has been performed on Ti substrate and the metallic material was detached and used for examinations. Table 3 presents the influence of the DC and PC conditions on the Sn, Cu and Ni content in the deposit and on its melting temperature.

It could be noticed an increase of the Ni content under PC plating from ~0.22 % to about 1.02 % as the applied frequency was reduced from 16.67 Hz (Sn-Cu-Ni-P1 system) towards 0.167 Hz (Sn-Cu-Ni-P3). Further decrease of the frequency up to 0.0167 Hz did not produce substantial changes in the elemental content of Ni that slightly decreased to 0.91 %. A relatively similar trend was observed in the case

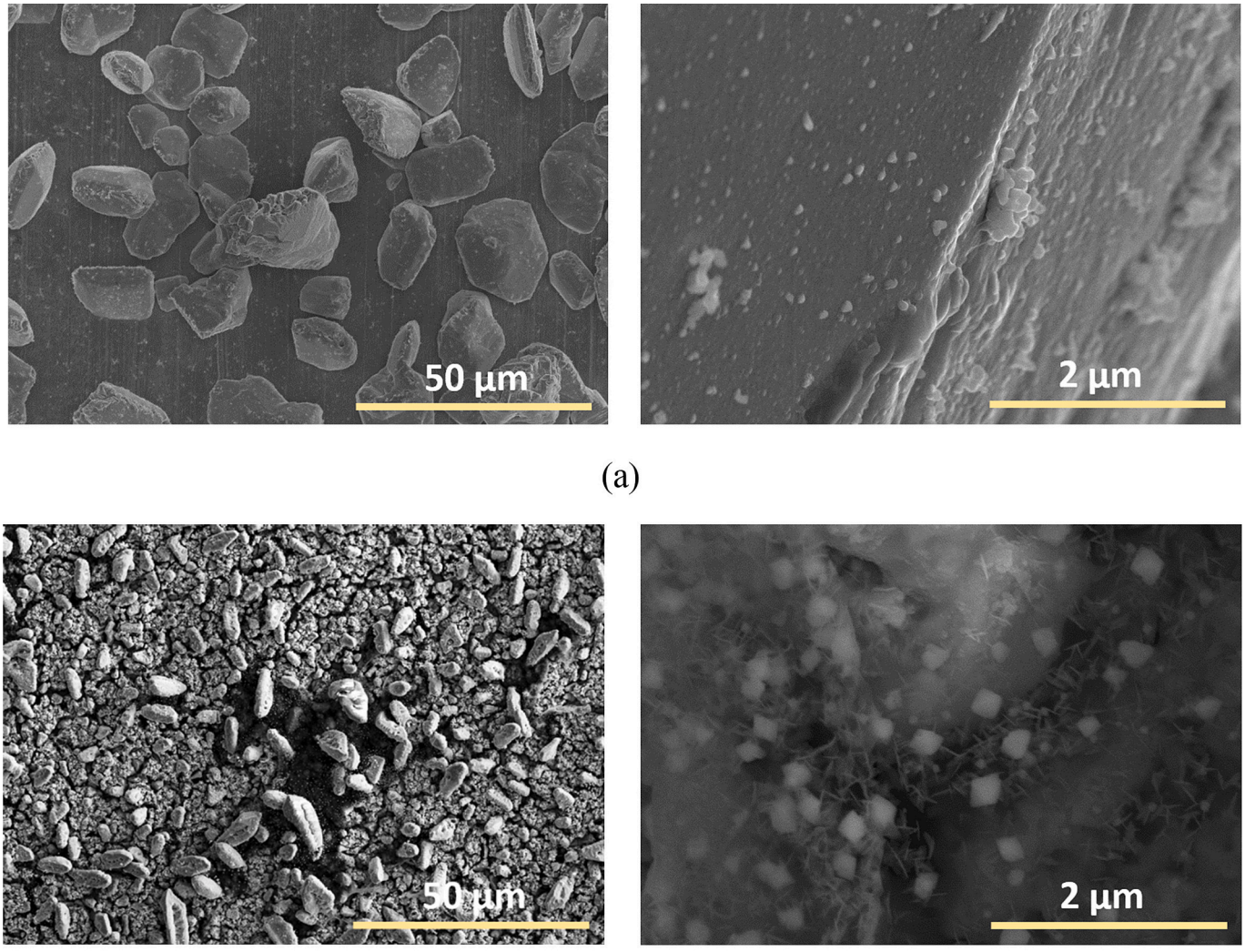

Fig. 9. SEM images at different magnifications of: (a) Sn-Cu-Ni-DC and (b) Sn-Cu-Ni-P2 after 24 h of immersion in 0.1 M NaCl electrolyte.

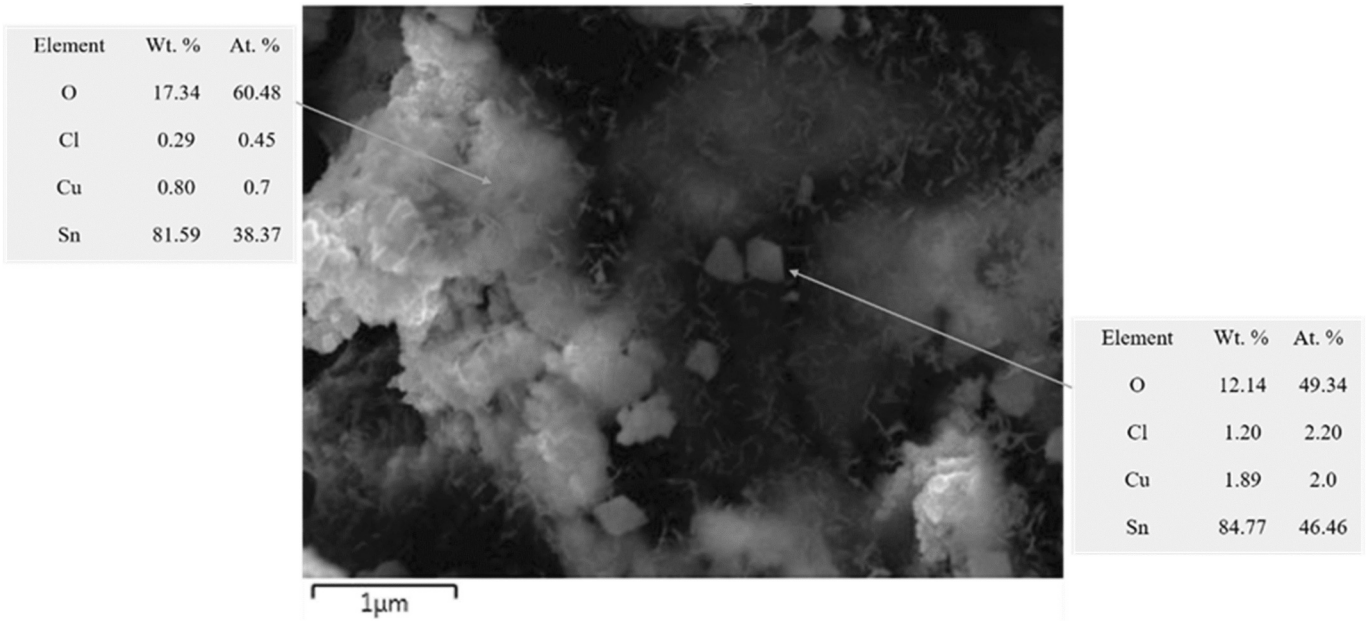

Fig. 10. Surface morphology and the corresponding EDX spectra of Sn-Cu-Ni-P2 sample after 24 h of immersion in 0.1 M NaCl electrolyte.

of Cu content: its value increased from about 0.44 % at frequencies in the range 16.67–1.667 Hz up to approximately 1.40 % at 0.0167 Hz.

The DSC curves recorded for the investigated ternary alloy deposits obtained under DC and PC conditions are presented in Fig. 3. A single endothermic peak could be evidenced on DSC curve for each sample composition. As shown in Fig. 3 and Table 3, the changes noticed in the alloy composition determine a modification of the melting temperature. Among all the electrodeposited alloys, it is noticed that the ones exhibiting higher Sn content present higher melting points. The small changes observed in the melting temperature values of the alloy deposits under DC and PC conditions are related to the slight variation of the Cu and Ni concentrations. Under PC conditions, the concentration of Cu and Ni slightly increase while varying the plating parameters This rising trend could be associated to the deposition mechanism.

It is well known that the use of pulsating current rather than a direct current provides additional possibilities to influence the alloy composition [46]. During PC electrodeposition, the Nerst-Diffusion layer is divided into two regions, namely a pulsating diffusion layer and a stationary one. By varying the frequency of the pulsating current, the concentration of the active species that will be reduced in the pulsating layer is modified [47]. The content of Cu in Sn-Cu deposits obtained from aqueous bath under pulse current plating mode (duty cycle = 9 %, Ton = 0.001 s and Toff = 0.01 s) varied with the applied current density [27]. It was noticed that the content of copper in the alloy decreases from 2.10 wt% to 0.70 wt% as the applied current density rise from 5 to 15 mA/cm^2. The increase in the current density resulted in the substantial reduction of Sn ions at the cathode, while a depletion of Cu ions occurs due to a lower limiting current density of Cu electrodeposition relative to Sn, considering the very high concentration of tin in the plating bath. In another investigation conducted by Han et al. [45] higher values of the Cu content in Sn-Cu alloy have been found when PC conditions were applied compared to DC plating mode when the alloy was electrodeposited from a chloride-citrate aqueous solution. Furthermore, Pallaro et al. [31] reported Sn-Cu alloys electrodeposited under PC plating mode from a deep eutectic solvent electrolyte with copper concentrations varying from 0.95 wt% to 4.3 wt% depending on the plating parameters. In our work, in the DES investigated electrolyte at 60 °C, the reduction potential of Sn^{2+} ions to Sn metal (−0.48 V *vs.* Ag ref.) is more noble than the potentials for the reduction of corresponding ions to Ni (−0.82 V *vs.* Ag ref.) and Cu (−0.86 V *vs.* Ag) [24]. Moreover, the concentrations of Cu and Ni cationic species chosen by us in the electrolyte are significantly lower as compared to that of Sn ones. Under these conditions, the electrodeposition of Sn is dominant. As the T_{ON} period is longer, the Sn^{2+} ions concentration becomes depleted near the cathode surface and more Cu and Ni metals are deposited during the "on-time" at low applied frequency pulse [16,45].

The XRD patterns of Sn-Cu-Ni alloys electrodeposited on the copper substrate under DC and various PC electrodeposition conditions are illustrated in Fig. 4. To better evidence the low-intensity peaks, the vertical axis has been presented using a logarithmic scale. No broad diffraction peaks could be observed in the X-ray patterns, suggesting a good crystallinity of the alloy deposits.

The phase composition of the alloy deposits electrochemically prepared under DC and PC conditions is relatively similar. The peaks attributed to tetragonal tin (card No. 00-004-0673) as the main alloying component and the copper (from both deposit and substrate, card No. 0 0-0 04-0836) are clearly evidenced. In addition, the peaks assigned to the monoclinic Cu_6Sn_5 (card No. 01-076-2703), hexagonal $(Cu,Ni)_6Sn_5$ (PCD Crystal Data #1905144) and cubic $CuNi_2Sn$ (ICSD#103068) intermetallic compounds have been found [23,48,49]. In the case of Sn-Cu-Ni-P2 and Sn-Cu-Ni-P3 systems, where the Ni content is higher than that of Cu, the peaks corresponding to $(Cu,Ni)_6Sn_5$ intermetallic are more pronounced. Ni could facilitate a partial conversion of Cu_6Sn_5 intermetallic compound phase into $(Cu,Ni)_6Sn_5$ phase [49]. Under very low applied pulse frequency (Sn-Cu-Ni-P4 system), the higher Cu content in the deposit determined more Cu_6Sn_5 compound to be formed, as suggested by the stronger intensity of the peaks corresponding to this phase.

3.2. *Corrosion behaviour of Sn-Cu-Ni alloys electrodeposited under DC and PC conditions*

3.2.1. *Potentiodynamic polarization and EIS*

To obtain further insights into the corrosion performance of the electrodeposited Sn-Cu-Ni alloy involving DC and PC plating conditions, a comparative electrochemical characterization has been performed at macro- and micro- scale in NaCl solution (0.5 M and 0.1 M). Different electrochemical techniques were involved and are further discussed. It should be mentioned that Sn-Cu-Ni-P2 has been selected as representative for PC electrodeposition conditions. The selection has been made

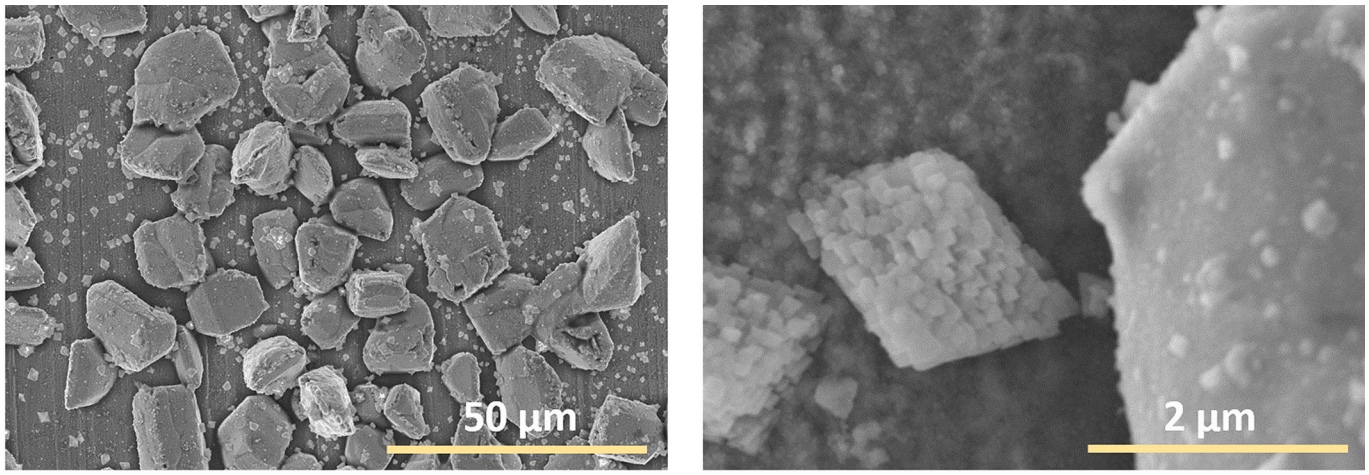

(a)

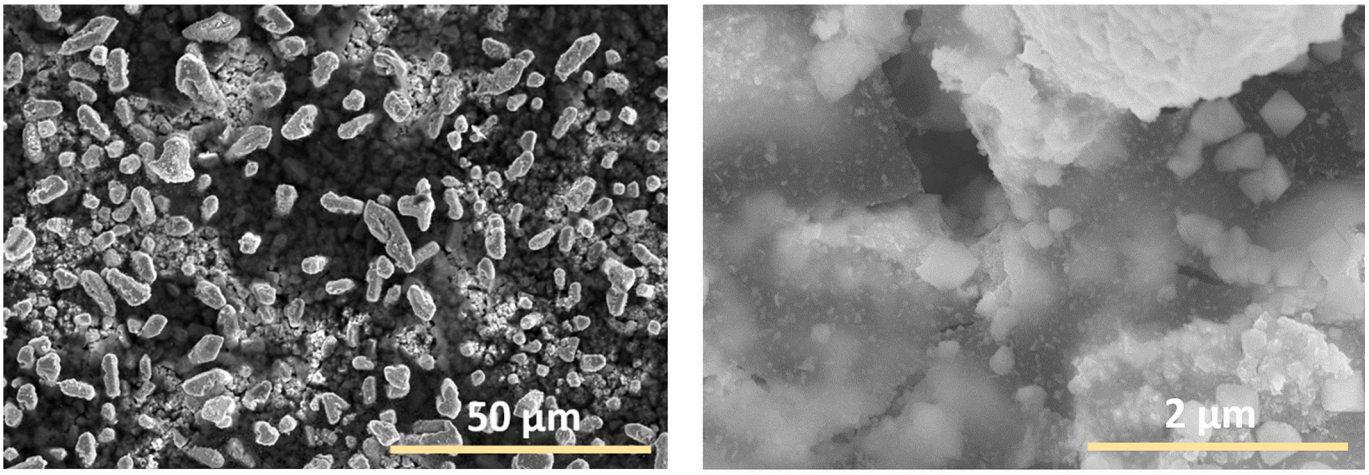

(b)

Fig. 11. SEM images at different magnifications of: (a) Sn-Cu-Ni-DC and (b) Sn-Cu-Ni-P2 after 168 h of immersion in 0.1 M NaCl electrolyte.

considering the grain size and the current efficiency. Among the different samples synthetized under PC, Sn-Cu-Ni-P2 presents an optimal balance between gain size and current efficiency. In addition, its melting point is close to the average value for PC condition.

Fig. 5 illustrates the typical polarization curves recorded in 0.5 M NaCl solution, represented in semilogarithmic coordinates, for the electrodeposited Sn-Cu-Ni alloys under both DC and PC plating conditions.

The anodic curves exhibit an increase of the current with potential, suggesting a uniform corrosion mechanism, related to the alloy dissolution. On scanning towards the anodic direction, three different potential ranges of polarization curve can be distinguished, illustrating the most important corrosion characteristics. In the first region there is a significant increase in the current density due to active dissolution of Sn-Cu-Ni alloy. The metal electrooxidation for sample prepared in PC conditions is more abrupt, suggesting that localized corrosion occurred, compared to sample prepared under DC mode which exhibits a typical uniform corrosion process. The active corrosion can be explained by predominant dissolution of Sn which is the major component of the alloy. Since alloy grains mainly containing tin are in contact with the copper metal from the substrate and the standard electrode potential of Sn/Sn^{2+} is more negative than of Cu/Cu^{2+} couple, tin will act as an anode in the galvanic cell and will be corroded preferentially. The copper and nickel as other alloy constituents do not influence the corrosion reaction since they are present in small concentration [12,50]. In the second part of polarization curve, the decrease of current after reaching a maximum value indicates a passive film formation. Some of the tin ions that pass through the aqueous solution will be adsorbed on the sample surface forming a corrosion protective layer. The characteristic potential is referred to as the passivation potential (E_p) and its value was shifted more negative (−0.288 V) for sample prepared by PC electrodeposition than in DC conditions (−0.164 V). The maximum recorded current density is referred to as the passivation current density (i_p) and a value of *ca* 3 mA/cm^2 was measured for both samples. We noticed that in this passivation region the current decreased with an order of magnitude. However, its value (0.51 mA/cm^2) for sample obtained by DC was found to be in a very narrow passive region, whereas the sample prepared in pulse has lower value (0.40 mA/cm^2) but almost independent of the potential on a larger potential domain. The passivation process may be explained by the formation of metal oxide precipitate on the electrode surface due to reaching a critical concentration of metal ions. Two different passive films may appear for the sample prepared in pulse conditions since the current density increases again (to 1.46 mA/cm^2) after the first passive region. The second passive film may

Element	Wt. %	At. %
O	14.79	54.55
Cl	0.39	0.65
Cu	6.09	5.66
Sn	78.73	39.15

Element	Wt. %	At. %
O	8.55	31.89
Cl	0.22	0.37
Cu	50.17	47.10
Sn	41.05	20.63

Element	Wt. %	At. %
O	9.44	43.19
Cl	0.12	0.26
Cu	1.42	1.64
Sn	89.01	54.91

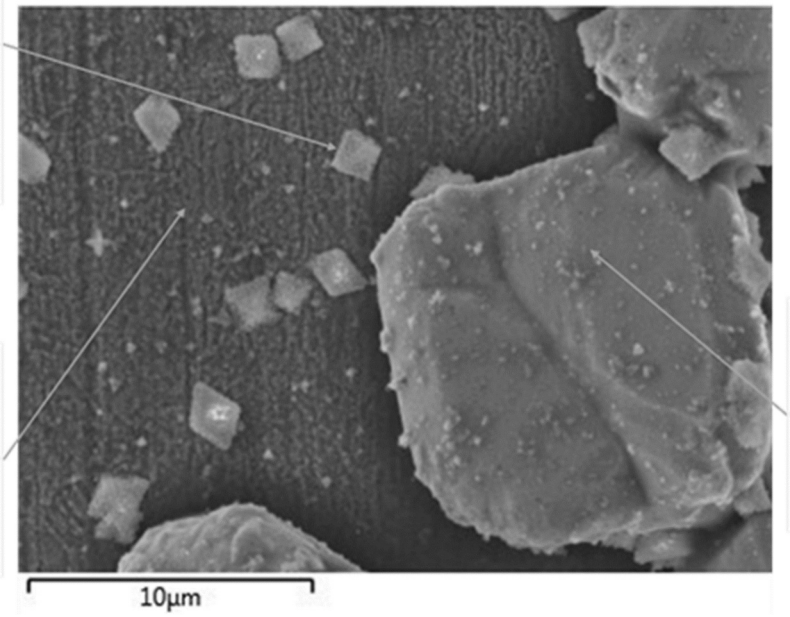

Fig. 12. Surface morphology and the corresponding EDX spectra of Sn-Cu-Ni-DC sample after 168 h of immersion in 0.1 M NaCl electrolyte.

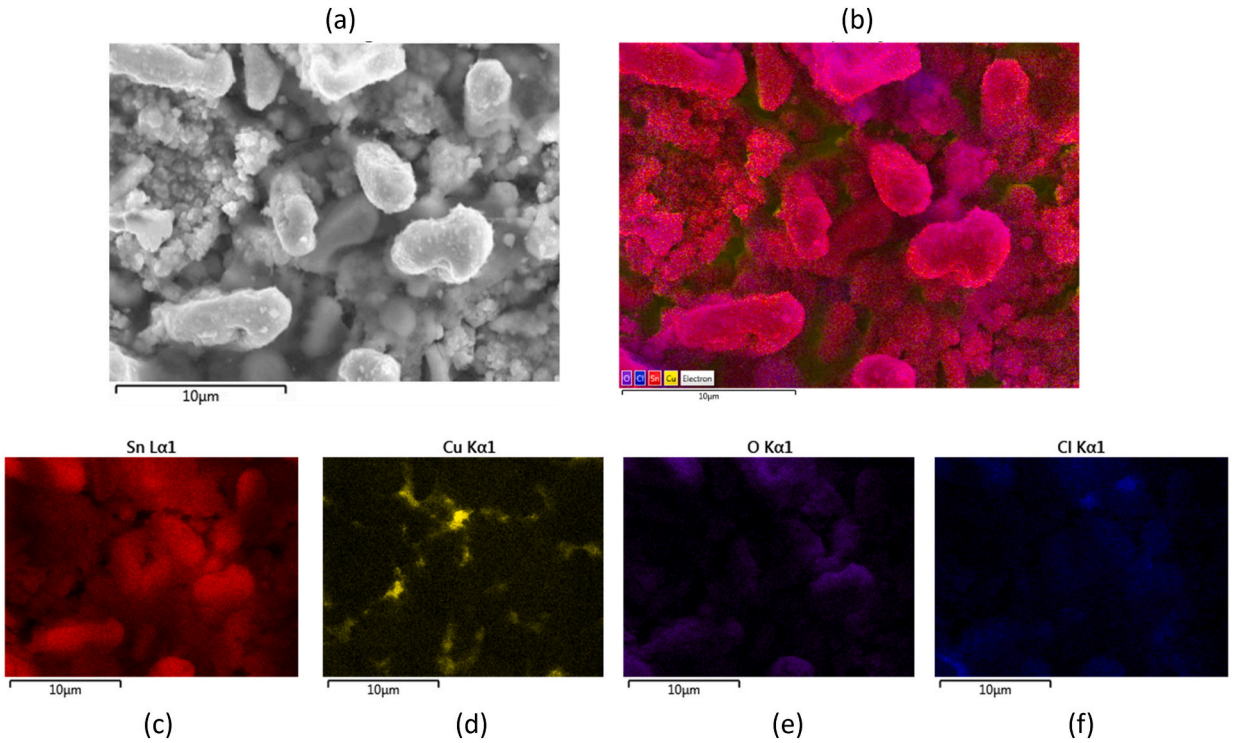

Fig. 13. Surface analysis (a) and the corresponding EDX qualitative maps (b, c, d, e, f) showing the distribution profiles of the significant elements in the case of Sn-Cu-Ni-P2 sample after 168 h of immersion in 0.1 M NaCl electrolyte.

be deposited directly on exposed Cu substrate since it occurs in a similar region as for DC sample where more substrate surface area is exposed. On further scanning, the third potential region can be seen more clearly after +0.1 V polarization, and it is assigned to the breakdown of the passive oxide layer due to the aggressive attack of Cl^- ions. The explanation of passivation and resumption of corrosion processes is consistent with the findings in literature [12,50,51].

The cathodic branch of the polarization curve of Sn-Cu-Ni-P2 alloy deposit shows a region up to around −0.80 V *vs.* Ag/AgCl evidencing a slow increase of the current, often linked to the oxygen reduction reaction. At more negative potentials, the hydrogen evolution reaction takes place, which is characterized by a distinct cathodic slope on the polarization curve [32,52]. In the case of Sn-Cu-Ni-DC deposit, a continuous increase of the cathodic current is observed, also presenting higher values than those of Sn-Cu-Ni-P2 at more negative potentials.

The corrosion potential (E_{corr}) and the corrosion current density

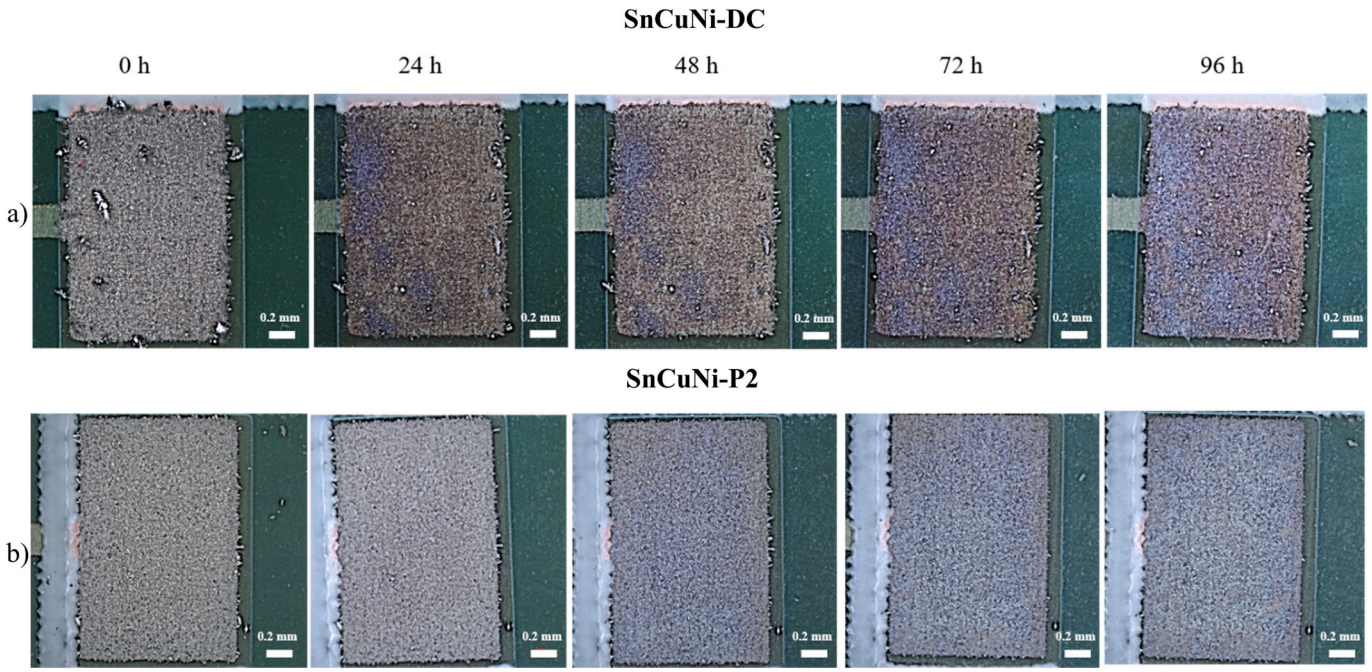

Fig. 14. Optical microscope images of PCBs covered with Sn-Cu-Ni alloys electrodeposited under (a) DC and (b) PC modes at different exposure periods during salt spray tests.

(i_{corr}) values for the two investigated specimens have been obtained by Tafel extrapolation. The Sn-Cu-Ni alloy deposit obtained under DC plating conditions exhibited an E_{corr} value of −0.628 V *vs.* Ag/AgCl while the use of PC conditions (Sn-Cu-Ni-P2 sample) determined its slight shifting towards more electropositive values, of about −0.604 V *vs.* Ag/AgCl. Correspondingly, the i_{corr} value for the specimen prepared under direct current conditions (Sn-Cu-Ni-DC) was 9.6 μA cm^{-2} whereas for the sample prepared using pulsed current (Sn-Cu-Ni-P2) a lower i_{corr} value 2.7 μA cm^{-2} was determined. By converting the determined corrosion current densities to corrosion rates (CR) expressed in mm/year, also considering the composition of the analysed specimens, values of 0.24 mm/year and of 0.07 mm/year for Sn-Cu-Ni-DC and Sn-Cu-Ni-P2 respectively have been obtained. The improved corrosion performance of the alloy deposits obtained under PC plating conditions could be attributed to their morphology. Hence, the relatively higher corrosion currents of less compact Sn-Cu-Ni-DC coatings would be explained due to the penetration of chloride ions through the gaps between the grains (as shown in Figs. 1 and 2). Furthermore, the cathode-to-anode ratio in the galvanic coupling between Sn, which is the major component of the alloy, and the copper for the substrate, influence the rate of corrosion. Image J software was utilized to analyse the SEM images, determining the ratio between uncovered areas with grains (cathode) and covered areas (anode) for both systems ($A_{uncovered}/A_{covered}$). Values of 0.9 ± 0.200 and 0.05 ± 0.006 were determined for Sn-Cu-Ni-DC and Sn-Cu-Ni-P2, respectively. Since the cathode-to-anode ratio is lower for the Sn-Cu-Ni-P2 system, it indicates a lower galvanic coupling and therefore lower corrosion rate, as previously determined. Regarding the intermetallic compounds, they are nobler than Sn and will serve as cathode, driving the dissolution of Sn phase [53,54].

Fig. 6 comparatively illustrates the EIS spectra of Sn-Cu-Ni ternary alloy synthesized under DC and PC plating conditions, in 0.5 M NaCl solution. Both Nyquist diagrams presented in Fig. 6a display a semicircle arc in the relatively high-frequency range. Their diameters are linked to the polarization resistance and could be connected to the corrosion rate. An observed increase in the semicircle diameter for the Sn-Cu-Ni-P2 sample indicates enhanced corrosion resistance in comparison to the Sn-Cu-Ni-DC sample. In addition, the lack of any supplementary straight line following the semicircle demonstrates that the formed passive films are not stable. Bode plots (Fig. 6b) also exhibit a quite similar shape, with the values of phase angle maximum for Sn-Cu-Ni-P2 and Sn-Cu-Ni-DC specimens at around −67.2° and −62.2°, respectively, meaning less electrically insulating products of corrosion and less homogeneous nature of the alloy deposit obtained under DC plating conditions.

The anticorrosive properties of Sn-Cu-Ni ternary alloy in sodium chloride can be described using a model consisting of a double layer capacitor (C_{dl}) in parallel with a charge-transfer resistor (R_{CT}). The charge-transfer resistor is related to the corrosion oxide product formed at the interface with solution, and it is in series with a second circuit comprising a film capacitor (C_F) in parallel with a film resistor (R_F) associated to the oxide layer/alloy interface. All these components are in series with the solution resistance (Rs), as presented in the inset of Fig. 6a. Regarding the fitting analysis, constant phase elements (CPE) were employed in place of true capacitances [24,32]. This choice was made to consider the non-ideal behaviour of capacitors. The EIS parameters for the proposed electrical equivalent circuit are showed in Table 4.

In the mathematical equation of CPE impedance, the variable "*n*" corresponds to the exponent. When $n = 1$, it represents pure capacitance, and when $n = 0$, it signifies pure ohmic resistance. In addition, it could be also associated with possible surface defects [32,55]. Observed values of both resistances and capacitances exhibit the typical order of magnitude. Yet, the values of $n_{(CPE\ 1)}$ ranging from 0.6 to 0.62 indicate a significant deviation from the ideal capacitance of the electrochemical double layer. On the other hand, the values of $n_{(CPE\ 2)}$ being very close to 1 suggest a nearly ideal behaviour of the film capacitance. The chi-square goodness-of-fit χ^2 related to error percentage between measurements and simulations has value of usual order of magnitude.

The experimental data of the film resistance $R_{F,}$ with values of about 12.2 kΩ cm^2 in the case of Sn-Cu-Ni-P2, and about 7.5 kΩ cm^2 for Sn-Cu-Ni-DC, are consistent with the polarization curves data, evidencing the positive influence of the PC plating conditions on the corrosion resistance of electrodeposited Sn-Cu-Ni alloy.

3.2.2. *Scanning vibrating electrode technique (SVET)*

The images capture through optical microscopy were associated with the ionic current density maps acquired during the use of scanning

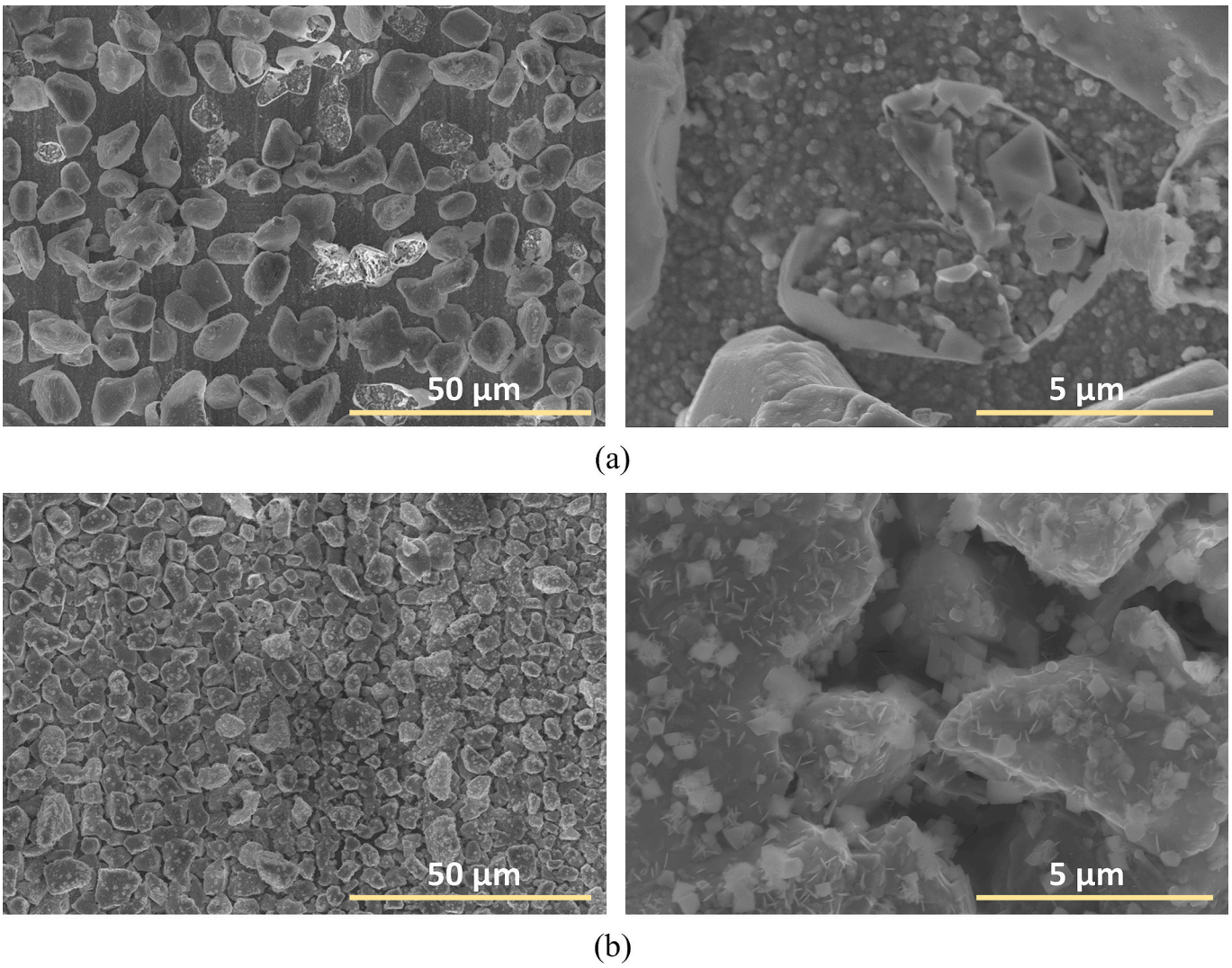

Fig. 15. SEM images at different magnifications of: (a) Sn-Cu-Ni-DC and (b) Sn-Cu-Ni-P2 after 96 h of exposure to salt-spray tests.

vibrating electrode technique (SVET) for Sn-Cu-Ni-DC and Sn-Cu-Ni-P2 as representative specimens, are presented in Figs. 7 and 8, respectively. The samples have been immersed in 0.1 M NaCl solution for a period of 168 h (one) and the current density maps have been recorded for the initial moment, after 24 h and 168 h of exposure to the aggressive solution. SVET is able to provide more details related to the localized processes of corrosion and galvanic coupling between tin as the main constituent of the alloy and copper, mainly from the substrate.

Both investigated specimens exhibit evidence of anodic and cathodic processes on their surfaces. The anodic activity is linked to the dissolution of the metallic grains, primarily containing tin, while the cathodic current is attributed to the electroreduction reaction of dissolved oxygen in the neutral aqueous solution [56]. A noticeable difference was observed as the immersion period increased. The values of the integrated anodic and cathodic currents I measured by SVET for different immersion periods are presented in Tables 5 and 6 for the two investigated specimens. They were determined according to the following Eq. (7.4) [57]:

$$\mathrm{I} = \int_0^x \int_0^y i_{xy}\mathrm{dx\ dy} = \sum i_{xy} A_0 \tag{7.4}$$

where i_{xy} is the current density determined by SVET measurements on each grid element having an area A_0.

As shown in Table 5, the Sn-Cu-Ni-DC specimen exhibited an increase of the integrated anodic current after 24 h of exposure in the aggressive 0.1 M NaCl solution, while after 168 h the I value decreased. On the contrary, in the case of the Sn-Cu-Ni-P2 specimen, a continuous decrease of the integrated anodic current values during the exposure was noticed (see Table 6). In addition, the lowest values of the integrated cathodic currents were observed for the Sn-Cu-Ni-P2 specimen, in a good agreement with the shape of cathodic branch of the polarization curve from Fig. 5.

Further inspection of the specimens by SEM associated with EDX analysis has been performed after 24 and 168 h of immersion in 0.1 M NaCl, as illustrated in Figs. 9–13.

Fig. 9 shows the SEM images of the investigated samples after 24 h of conditioning. After immersing the Sn-Cu-Ni-DC specimen for 24 h, no corrosion products are observed on its surface (Fig. 9a), while in the case of Sn-Cu-Ni-P2 one the formation of crystals and spongeous plate-like corrosion products were noticed (Fig. 9b). The corresponding EDX analysis on the corrosion products of Sn-Cu-Ni-P2, as illustrated in Fig. 10, shows Sn, O, Cu and Cl elements, suggesting the formation of compounds composed of tin oxides and chlorides [34]. The formation of SnO_2/SnO crystals has also been observed by Wang et al. [58,59], as well as of complex oxide chloride hydroxide of Sn, when SAC305 solder joint was exposed to aggressive environments. Due to the nobler nature of Cu compared to Sn, it could act as a cathode, promoting the corrosion of tin phase resulting in the formation SnO_2/SnO crystals as the galvanic

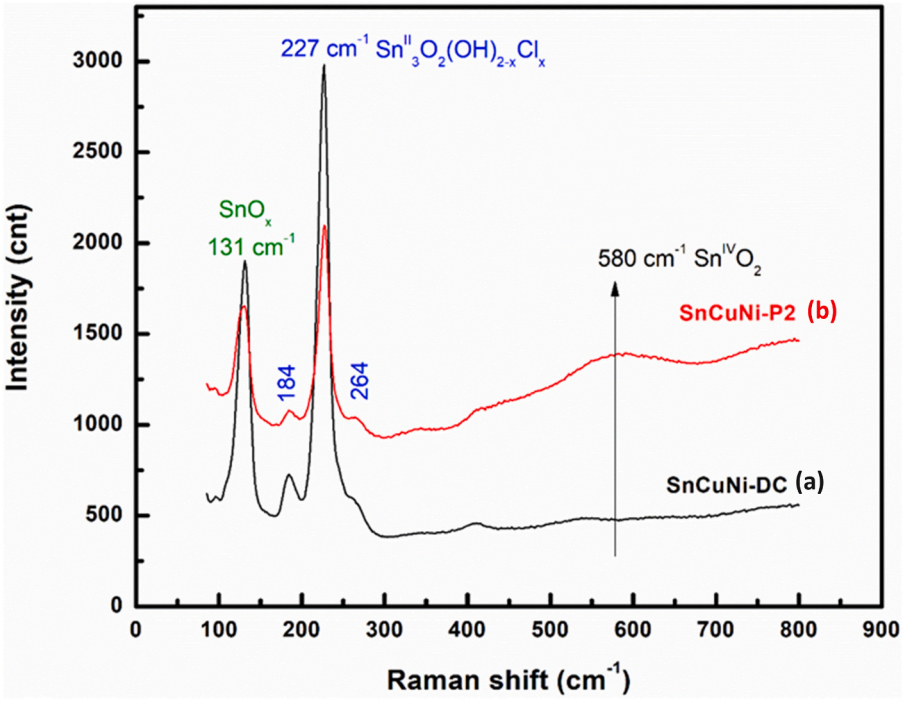

Fig. 16. The Raman spectra for: (a) Sn-Cu-Ni-DC and (b) Sn-Cu-Ni-P2 specimens after 168 h of immersion in 0.1 M NaCl electrolyte.

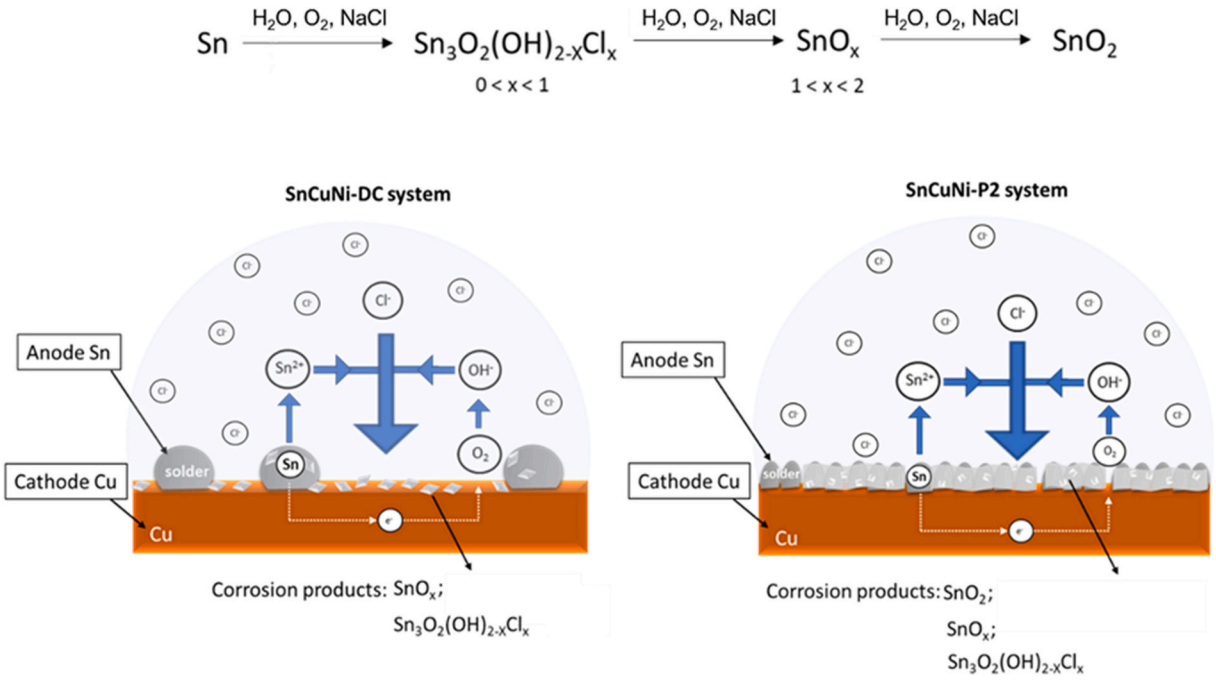

Fig. 17. Reaction sequence and the graphical representation of the proposed corrosion mechanism for both Sn-Cu-Ni-DC and Sn-Cu-Ni-P2 systems.

cell reaction products of tin corrosion. Therefore, the decrease in the anodic corrosion current observed on SVET map of the Sn-Cu-Ni-P2 system after 24 h of immersion may be linked to the formation of corrosion products on the surface of the sample, as it was revealed by the SEM-EDX analysis.

Fig. 11 illustrates the surface morphology of Sn-Cu-Ni-DC and Sn-Cu-Ni-P2 specimens after 168 h of conditioning in 0.1 M NaCl solution. As shown in Fig. 11, the presence of the corrosion products could be clearly evidenced on both specimens. In addition, the EDX investigations presented in Figs. 12 and 13 revealed Sn, O, Cu and Cl elements in the corrosion products.

The corrosion products formed onto the Sn-Cu-Ni-DC specimen show a crystal-like morphology randomly distributed over the surface, quite similar to that noticed on Sn-Cu-Ni-P2 one after 24 h of immersion, however exhibiting larger crystal sizes (see Fig. 11a). In the case of Sn-Cu-Ni-P2 specimen, the film initially formed after 24 h of exposure has become more compact as the conditioning period was longer, covering almost the entire surface, as revealed in Fig. 11b.

Corrosion products presenting crystal shape morphology are still detected on the surface of Sn-Cu-Ni-P2 specimen. In addition, some

regions show a breaking of the corrosion products film, exposing the Cu metallic substrate (see Fig. 13). A quite similar morphology has been presented by Guerrero et al. [12] during the leaching of Sn-0.7Cu-0.05Ni solder and joint on Cu substrate in 3.5 wt% NaCl solution.

3.2.3. Salt mist tests

Printed circuit boards (PCBs) specimens were electrochemically coated with Sn-Cu-Ni ternary alloys under DC and PC plating conditions and were exposed to salt-spray tests for 96 h, to gather additional insides regarding the anti-corrosive properties of the alloy. Every 24 h the pads on the PCBs were examined using an optical microscope, as presented in Fig. 14. In the case of the deposits applied using PC conditions, the optical inspection did not reveal significant surface modifications during the entire test period. On the contrary, for PCBs coated with Sn-Cu-Ni ternary alloy under DC conditions, after 24 h of exposure there are signs of corrosion attack, that became more prominent as the exposure period was longer.

Fig. 15 shows the SEM micrographs of the Sn-Cu-Ni ternary alloys following 96 h of exposure to aggressive environment. Considering the alloy prepared under DC mode, the corrosion attack is primarily focused on the irregular grains, as could be seen in Fig. 15a. As the alloy's primary constituent is Sn it acts as an anode in the galvanic couple with the Cu substrate and drove the preferential dissolution of the grains. The corrosion products exhibiting crystal like morphology were not observed on the surface, as in the immersion experiments, probably due to their poor adhesion under salt-spray conditions. For Sn-Cu-Ni-P2 specimens, even after 96 h of exposure, crystals and spongeous plate-like corrosion products are observed partially covering the surface of the sample (Fig. 15b). The EDX analysis (not shown here) indicates the presence of O, Cl, and Sn, suggesting the formation of tin oxides and chlorides corrosion products. They may act as a physical barrier, impeding the access of corrosive species from the environment, which in turn reduces the corrosion rate [60].

3.2.4. Raman analysis of the corrosion products

Raman spectroscopy was used to evaluate the nature of the corrosion products in the examined samples after 168 h of exposure in 0.1 M NaCl, see Fig. 16. The spectra's were correlated with the data from the literature. Therefore, the peaks positioned at 184, 227 and 264 cm^{-1} could be associated to the complex tin oxi-hydroxy-chloride $Sn^{II}_3O_2(OH)_{2-x}Cl_x$ ($0 < x < 1$) while the one at 131 cm^{-1} could be attributed to a transition oxide phase SnO_x ($1 < x < 2$) [61–63]. In addition, for the Sn-Cu-Ni-P2 specimen a supplementary Raman broad signal is evidenced in the range 470–680 cm^{-1} which may be assigned to amorphous $Sn^{IV}O_2$ species [62].

Considering all above-mentioned results, the suggested reaction pathway for the generation of the corrosion products as well as the mechanism of corrosion of Sn-Cu-Ni-DC and Sn-Cu-Ni-P2 samples are illustrated in Fig. 17.

As Sn is the primary constituent of the alloy, it will behave as the anode in the galvanic coupling with Cu from the substrate. This is due to Sn having a less positive corrosion potential than Cu, which serves as the cathode in the system. Also, the intermetallic compounds will act as cathode since they are nobler than Sn and promote its dissolution. The dissolution of Sn will lead to the formation of Sn^{2+} ions in the aggressive environment. Subsequently, Sn^{2+} ions will undergo a reaction with the hydroxide ions produced from the oxygen reduction reaction that occurs at the cathode, resulting in the formation of tin hydroxide species. The high content of chloride ions in the environment, will transform the hydroxide compounds into $Sn_3O_2(OH)_{2-x}Cl_x$ species, which will further convert into tin oxide compounds [61–64]. Raman spectroscopy revealed the presence of SnO_2 as final corrosion product only in the sample prepared under pulsed plating mode.

4. Conclusions

The performed investigations analysed the morphology, composition and the corrosion performance of Sn-Cu-Ni ternary alloys synthesized by electrodeposition under direct (DC) and pulse (PC) current plating conditions from a DES based-electrolyte consisting in choline chloride: ethylene glycol (1:2 molar ratio). To the best of our knowledge, this is the first report in literature dealing with the pulse plating of Sn-Cu-Ni alloys from deep eutectic solvents and with their corrosion performance evaluation involving SVET. From the results obtained, the following conclusions are withdrawn:

1. The use of PC conditions facilitated the formation of more compact alloy deposits as compared to those prepared under DC ones. A decrease of the grain size is produced as the pulse frequency is lower. Lower melting temperatures of the alloys were determined when pulsed current is applied, associated with the changes of their chemical composition.
2. Potentiodynamic polarization analysis in 0.5 M NaCl solution indicated lower corrosion currents for the ternary alloy obtained under pulsed current mode (Sn-Cu-Ni-P2 system) compared to the deposit obtained under DC plating conditions.
3. Micro-scale corrosion investigations using SVET during continuous immersion for 168 h in 0.1 M NaCl showed a decrease of the anodic current for the Sn-Cu-Ni alloy deposits, regardless the involved current form during electrochemical preparation.
4. Salt-spray test analysis on PCBs covered with Sn-Cu-Ni alloy under DC and PC modes, showed that PC electrodeposition conditions leads to enhanced anticorrosive properties of the deposits due to the formation of adherent corrosion products on the surface.
5. The corrosion products on the samples were investigated by SEM, EDX and Raman analysis. Based on the results obtained, a corrosion mechanism has been proposed. As Sn is the predominant element of the solder alloy, the corrosion and dissolution processes predominantly take place at Sn. Upon generation, Sn^{2+} ions react with the hydroxide ions, resulted from the oxygen reduction reaction at the cathode, producing tin hydroxide species. The high content of chloride ions in the environment will transform the hydroxide compounds into $Sn_3O_2(OH)_{2-x}Cl_x$ species which subsequently converts into tin oxide compounds.

CRediT authorship contribution statement

Sabrina Patricia State: Formal analysis, Investigation, Writing – original draft, Writing – review & editing, Visualization. **Stefania Costovici:** Conceptualization, Formal analysis, Investigation, Methodology, Validation. **Mirsajjad Mousavi:** Formal analysis. **Yaiza Gonzalez Garcia:** Formal analysis, Supervision, Writing – original draft. **Caterina Zanella:** Investigation, Supervision, Writing – original draft. **Anca Cojocaru:** Project administration, Writing – original draft. **Liana Anicai:** Conceptualization, Data curation, Methodology, Supervision, Validation, Writing – original draft, Writing – review & editing. **Teodor Visan:** Supervision, Validation, Writing – original draft. **Marius Enachescu:** Project administration, Resources, Supervision.

Declaration of competing interest

The authors declare that they have no known competing financial interests or personal relationships that could have appeared to influence the work reported in this paper.

Data availability

No data was used for the research described in the article.

Acknowledgements

This research work was funded by the European Union's Horizon 2020 - Research and Innovation Framework Programme under the H2020 Marie Skłodowska-Curie Actions, grant number 764977; and by the Ministry of Education and Research, Romania under NOVTI-NALBEST project 38/2016, M Era Net Program; and by ECSEL JU under the following grant agreement No. 876124 (BEYOND5). The JU receives support from the European Union's Horizon 2020 research and innovation programme and Italy, Switzerland, Germany, Belgium, Sweden, Austria, Romania, Slovakia, France, Poland, Spain, Ireland, Israel, Portugal, Greece, Netherlands, Hungary, United Kingdom. This work is financially supported by the Romanian Ministry of Research, Innovation and Digitalization, under the following ECSEL - H2020 Project: BEYOND5 - Contract no. 12/1.1.3/31.07.2020, POC-SMIS code 136877.

References

[1] K.J. Puttlitz, G.T. Galyon, Impact of the ROHS Directive on high-performance electronic systems part II: key reliability issues preventing the implementation of lead-free solders, Lead-Free Electron, Solder. A Spec. Issue J. Mater. Sci. Mater. Electron. (2007) 347–365, https://doi.org/10.1007/978-0-387-48433-4_23.
[2] W. Tang, Y. Hu, S. Huang, Fabrication of Sn-Cu alloy solder by pulse electroplating on the metalized Si wafer, Met. Mater. Int. 18 (2012) 177–183, https://doi.org/10.1007/s12540-012-0022-1.
[3] S. Cheng, C.M. Huang, M. Pecht, A review of lead-free solders for electronics applications, Microelectron. Reliab. 75 (2017) 77–95, https://doi.org/10.1016/j.microrel.2017.06.016.
[4] X.W. Wenchao Yang, Du Zaixiang, Yu Shuyuan, Yitai Li, Q.L. Junli Feng, Y. Zhan, The effect of rare earths additions on the microstructure and the corrosion behavior of Sn-0.7Cu-0.075Al solder alloy, Materials (Basel) 12 (2019) 3731 (doi:1996-1944/12/22/3731).
[5] W.R. Osório, L.C. Peixoto, L.R. Garcia, N. Mangelinck-Noël, A. Garcia, Microstructure and mechanical properties of Sn-Bi, Sn-Ag and Sn-Zn lead-free solder alloys, J. Alloys Compd. 572 (2013) 97–106, https://doi.org/10.1016/j.jallcom.2013.03.234.
[6] T. Ventura, C.M. Gourlay, K. Nogita, T. Nishimura, M. Rappaz, A.K. Dahle, The influence of 0-0.1 wt.% Ni on the microstructure and fluidity length of Sn-0.7Cu-xNi, J. Electron. Mater. 37 (2008) 32–39, https://doi.org/10.1007/s11664-007-0281-7.
[7] K. Nogita, T. Nishimura, Nickel-stabilized hexagonal (Cu, Ni)6Sn5 in Sn-Cu-Ni lead-free solder alloys, Scr. Mater. 59 (2008) 191–194, https://doi.org/10.1016/j.scriptamat.2008.03.002.
[8] K. Seelig, T.O. Neill, K. Pigeon, M. Maaleckian, A. Monson, W. Machado, H. Industries, G. Controls, N. Kingstown, Production testing of Ni-modified SnCu solder paste. https://aimsolder.com/es/technical-articles/production-testing-ni-modified-sncu-solder-paste, 2013.
[9] K. Nogita, S.D. McDonald, H. Tsukamoto, J. Read, S. Suenaga, T. Nishimura, Inhibiting cracking of interfacial Cu6Sn5 by Ni additions to Sn-based lead-free solders, Trans. Jpn. Inst. Electron. Packag. 2 (2009) 46–54, https://doi.org/10.5104/jiepeng.2.46.
[10] K. Nogita, J. Read, T. Nishimura, K. Sweatman, S. Suenaga, A.K. Dahle, Microstructure control in Sn-0.7 mass% Cu alloys, Mater. Trans. 46 (2005) 2419–2425, https://doi.org/10.2320/matertrans.46.2419.
[11] H. Nishikawa, J.Y. Piao, T. Takemoto, Interfacial reaction between Sn-0.7Cu (-Ni) solder and Cu substrate, J. Electron. Mater. 35 (2006) 1127–1132, https://doi.org/10.1007/BF02692576.
[12] J.E.C. Guerrero, D.H. Camacho, O. Mokhtari, H. Nishikawa, Corrosion and leaching behaviours of Sn-0.7Cu-0.05Ni lead-free solder in 3.5 wt.% NaCl solution, Int. J. Corros. 2018 (2018), https://doi.org/10.1155/2018/6580750.
[13] T. Ventura, Y. Cho, A.K. Dahle, Solidification mechanisms in the Sn-Cu-Ni lead-free solder system, Mater. Sci. Forum 654–656 (2010) 1381–1384, https://doi.org/10.4028/www.scientific.net/MSF.654-656.1381.
[14] L. Snugovsky, P. Snugovsky, D.D. Perovic, J.W. Rutter, Phase equilibria in Sn rich corner of Cu-Ni-Sn system, Mater. Sci. Technol. 22 (2006) 899–902, https://doi.org/10.1179/174328406X109249.
[15] C. Schmetterer, H. Flandorfer, C. Luef, A. Kodentsov, H. Ipser, Cu-Ni-Sn: a key system for lead-free soldering, J. Electron. Mater. 38 (2009) 10–24, https://doi.org/10.1007/s11664-008-0522-4.
[16] Y. Goh, A.S.M.A. Haseeb, M.F.M. Sabri, Electrodeposition of lead-free solder alloys, Solder. Surf. Mount Technol. 25 (2013) 76–90, https://doi.org/10.1108/09540911311309031.
[17] H. Nawafune, Soldering in Electronics. Science, Technology and Environmental Impact, Chapter 4: plating lead-free soldering in electronics, Marcel Dekker Inc., 2004.
[18] M. Mallik, A. Mitra, S. Sengupta, K. Das, R.N. Ghosh, S. Das, Effect of current density on the nucleation and growth of crystal facets during pulse electrodeposition of Sn-Cu lead-free solder, Cryst. Growth Des. 14 (2014) 6542–6549, https://doi.org/10.1021/cg501440a.
[19] E.L. Smith, A.P. Abbott, K.S. Ryder, Deep e (DESs) and their applications, Chem. Rev. 114 (2014) 11060–11082, https://doi.org/10.1021/cr300162p.
[20] R. Holze, Electrodeposition from ionic liquids, in: F. Endres, A.P. Abbott, D. R. MacFarlane (Eds.), J. Solid State Electrochem, vol. 13(2009), WILEY-VCH, Weinheim, 2008, pp. 1633–1634, https://doi.org/10.1007/s10008-009-0821-6.
[21] A.P. Abbott, G. Frisch, K.S. Ryder, Electroplating using ionic liquids, Annu. Rev. Mater. Res. 43 (2013) 335–358, https://doi.org/10.1146/annurev-matsci-071312-121640.
[22] A.P. Abbott, G. Capper, D.L. Davies, R.K. Rasheed, Ionic liquid analogues formed from hydrated metal salts, Chem. Eur. J. 10 (2004) 3769–3774, https://doi.org/10.1002/chem.200400127.
[23] S. Rao, X. Zou, S. Wang, T. Shi, Y. Lu, L. Ji, H.-Y. Hsu, Q. Xu, X. Lu, Electrodeposition of porous Sn-Ni-Cu alloy anode for Lithium-ion batteries from nickel matte in deep eutectic solvents, J. Electrochem. Soc. 166 (2019) D427–D434, https://doi.org/10.1149/2.0881910jes.
[24] S.P. Rosoiu, S. Costovici, C. Moise, A. Petica, L. Anicai, T. Visan, M. Enachescu, Electrodeposition of ternary Sn-Cu-Ni alloys as lead-free solders using deep eutectic solvents, Electrochim. Acta (2021), 139339, https://doi.org/10.1016/j.electacta.2021.139339.
[25] W.E.G. Hansal, S. Roy, Pulse Plating, 1st editio, Leuze Verlag, 2012.
[26] J.C. Puippe, Guidelines for setting the useful range of pulse plating parameters, Trans. Inst. Met. Finish. 96 (2018) 244–252, https://doi.org/10.1080/00202967.2018.1501907.
[27] A. Sharma, B. Ahn, Pulse plated Sn-Cu solder coatings from stannate bath, Solder. Surf. Mount Technol. 32 (2020) 24–32, https://doi.org/10.1108/SSMT-08-2019-0027.
[28] S.P. Rosoiu, A.G. Pantazi, A. Petica, A. Cojocaru, S. Costovici, C. Zanella, T. Visan, L. Anicai, M. Enachescu, Comparative study of Ni-Sn alloys electrodeposited from choline chloride-based ionic liquids in direct and pulsed current, Coatings 9 (2019) 1–15, https://doi.org/10.3390/coatings9120801.
[29] S. Xing, C. Zanella, F. Deflorian, Effect of pulse current on the electrodeposition of copper from choline chloride-ethylene glycol, J. Solid State Electrochem. 18 (2014) 1657–1663, https://doi.org/10.1007/s10008-014-2400-8.
[30] L. Anicai, A. Petica, S. Costovici, C. Moise, O. Brincoveanu, T. Visan, Electrodeposition of Sn-In alloys involving deep eutectic solvents, Coatings 9 (2019) 1–14, https://doi.org/10.3390/coatings9120800.
[31] M. Pallaro, F.L. Moretto, G. Panzeri, L. Magagnin, Sn-Cu codeposition from a non-aqueous solution based on ethylene glycol for wafer-bonding applications: direct and pulse electroplating, Trans. Inst. Met. Finish. 96 (2018) 265–268, https://doi.org/10.1080/00202967.2018.1507329.
[32] W.R. Osório, E.S. Freitas, J.E. Spinelli, A. Garcia, Electrochemical behavior of a lead-free Sn-Cu solder alloy in NaCl solution, Corros. Sci. 80 (2014) 71–81, https://doi.org/10.1016/j.corsci.2013.11.010.
[33] S. Li, X. Wang, Z. Liu, Y. Jiu, S. Zhang, J. Geng, X. Chen, S. Wu, P. He, W. Long, Corrosion behavior of Sn-based lead-free solder alloys: a review, J. Mater. Sci. Mater. Electron. 31 (2020) 9076–9090, https://doi.org/10.1007/s10854-020-03540-2.
[34] Y. Gonzalez-Garcia, S.J. Garcia, J.M.C. Mol, Electrochemical Techniques for the Study of Self Healing Coatings, 2016, https://doi.org/10.1007/978-94-017-7540-3_9.
[35] A.C. Bastos, M.C. Quevedo, O.V. Karavai, M.G.S. Ferreira, Review—on the application of the scanning vibrating electrode technique (SVET) to corrosion research, J. Electrochem. Soc. 164 (2017) C973–C990, https://doi.org/10.1149/2.0431714jes.
[36] H.S. Isaacs, The measurement of the galvanic corrosion of soldered copper using the scanning vibrating electrode technique, Corros. Sci. 28 (1988) 547–558, https://doi.org/10.1016/0010-938X(88)90023-6.
[37] ASTM B117-2019: Standard Practice for Operating Salt Spray (Fog) Apparatus, ASTM International, United States, 2019 (n.d.).
[38] ISO 9227:2017 Corrosion Tests in Artificial Atmospheres—Salt Spray Tests, International Organization for Standardization, Geneva, Switzerland 2017, n.d.
[39] N. Ibl, Some theoretical aspects of pulse electrolysis, Surf. Technol. 10 (1980) 81–104, https://doi.org/10.1016/0376-4583(80)90056-4.
[40] S. Cinhagir, Powder Pulse Plating, University of Leicester, 2018.
[41] T. Green, X. Su, S. Roy, Pulse plating of copper from deep eutectic solvents, ECS Trans. 77 (2017) 1247–1253, https://doi.org/10.1149/07711.1247ecst.
[42] A. Ispas, A. Bund, Pulse plating of tantalum from 1-butyl-1-methyl-pyrrolidinium bis(trifluoromethylsulfonyl)amide ionic liquids, Trans. Inst. Met. Finish. 90 (2012) 298–304, https://doi.org/10.1179/0020296712Z.00000000058.
[43] R. Böck, G. Lanzinger, R. Freudenberger, T. Mehner, D. Nickel, I. Scharf, T. Lampke, Effect of additive and current mode on surface morphology of palladium films from a non-aqueous deep eutectic solution (DES), J. Appl. Electrochem. 43 (2013) 1207–1216, https://doi.org/10.1007/s10800-013-0608-4.
[44] A. Sharma, S. Bhattacharya, S. Das, K. Das, A study on the effect of pulse electrodeposition parameters on the morphology of pure tin coatings, Metall. Mater. Trans. A Phys. Metall. Mater. Sci. 45 (2014) 4610–4622, https://doi.org/10.1007/s11661-014-2389-8.
[45] C. Han, Q. Liu, D.G. Ivey, Electrodeposition of Sn-0.7 wt% Cu eutectic alloys from chloride-citrate solutions, Plat. Surf. Finish. 95 (2008) 21–29.
[46] P.D. Landolt, Fundamental aspects of alloy plating, Plat. Surf. Finish. 88 (2001) 70–79.
[47] A. Ispas, A. Bund, Electrodeposition in ionic liquids, Interface Mag. 23 (2014) 47–51, https://doi.org/10.1149/2.F05141if.
[48] A.A. El-Daly, A.E. Hammad, Enhancement of creep resistance and thermal behavior of eutectic Sn-Cu lead-free solder alloy by Ag and In-additions, Mater. Des. 40 (2012) 292–298, https://doi.org/10.1016/j.matdes.2012.04.007.
[49] A. El-Daly, S.A. Eladly, A. Mohamed, T.A. Elmosalami, M.S. Dawood, Improvement of strength-ductility trade-off in a Sn–0.7Cu–0.2Ni lead-free solder alloys through

Al-microalloying, J. Mater. Sci. Mater. Electron. 31 (2020) 8649–8661, https://doi.org/10.1007/s10854-020-03400-z.
[50] X.D. Lao, C.Q. Cheng, X.H. Min, J. Zhao, D.Y. Zhou, L.H. Wang, X.G. Li, Corrosion and leaching behaviors of Sn-based alloy in simulated soil solutions, Trans. Nonferrous Met. Soc. China (English Ed.) 26 (2016) 581–588, https://doi.org/10.1016/S1003-6326(16)64146-8.
[51] A. Gharaibeh, I. Felhősi, Z. Keresztes, G. Harsányi, B. Medgyes, B. Illés, Electrochemical corrosion of sac alloys: a review, Metals (Basel) 10 (2020) 1–18, https://doi.org/10.3390/met10101276.
[52] Y.F. Gao, C.Q. Cheng, J. Zhao, L.H. Wang, X.G. Li, Electrochemical corrosion of Sn-0.75Cu solder joints in NaCl solution, Trans. Nonferrous Met. Soc. China (English Ed.) 22 (2012) 977–982, https://doi.org/10.1016/S1003-6326(11)61273-9.
[53] E.S. Freitas, W.R. Osório, J.E. Spinelli, A. Garcia, Mechanical and corrosion resistances of a Sn-0.7 wt.%Cu lead-free solder alloy, Microelectron. Reliab. 54 (2014) 1392–1400, https://doi.org/10.1016/j.microrel.2014.02.014.
[54] S. Farina, C. Morando, Comparative corrosion behaviour of different Sn-based solder alloys, J. Mater. Sci. Mater. Electron. 26 (2015) 464–471, https://doi.org/10.1007/s10854-014-2422-0.
[55] A. Gupta, C. Srivastava, Electrodeposition current density induced texture and grain boundary engineering in Sn coatings for enhanced corrosion resistance, Corros. Sci. 194 (2022), 109945, https://doi.org/10.1016/j.corsci.2021.109945.
[56] R.M. Souto, Y. González-García, A.C. Bastos, A.M. Simões, Investigating corrosion processes in the micrometric range: a SVET study of the galvanic corrosion of zinc coupled with iron, Corros. Sci. 49 (2007) 4568–4580, https://doi.org/10.1016/j.corsci.2007.04.016.
[57] V. Cerveira, N.F. Lopes, L.F.P. Dick, Anomalous currents determined by SVET due to composition gradients on corroding Zn surfaces in 0.1 M NaCl, J. Solid State Electrochem. 24 (2020) 1889–1898, https://doi.org/10.1007/s10008-020-04646-7.
[58] M. Wang, J. Wang, W. Ke, Effect of microstructure and Ag3Sn intermetallic compounds on corrosion behavior of Sn–3.0Ag–0.5Cu lead-free solder, J. Mater. Sci. Mater. Electron. 25 (2014) 5269–5276, https://doi.org/10.1007/s10854-014-2300-9.
[59] M. Wang, J. Wang, W. Ke, Corrosion behavior of Sn-3.0Ag-0.5Cu lead-free solder joints, Microelectron. Reliab. 73 (2017) 69–75, https://doi.org/10.1016/j.microrel.2017.04.017.
[60] J.S. Cala, C.M. Miranda, D.L. Cataño, D.Y. Peña, H.S. Klapper, Role of corrosion products by the sulfidation of AISI/SAE-1020 steel in heavy crude oil at high temperatures, Chem. Eng. Trans. 57 (2017) 1435–1440, https://doi.org/10.3303/CET1757240.
[61] J.L. Gole, A.V. Iretskii, M.G. White, A. Jacob, W.B. Carter, S.M. Prokes, A. S. Erickson, Suggested oxidation state dependence for the activity of submicron structures prepared from tin/tin oxide mixtures, Chem. Mater. 16 (2004) 5473–5481, https://doi.org/10.1021/cm030618i.
[62] P. Eckold, M. Rolff, R. Niewa, W. Hügel, Synthesis, characterization and in situ Raman detection of Sn3O2(OH)2-xClx phases as intermediates in tin corrosion, Corros. Sci. 98 (2015) 399–405, https://doi.org/10.1016/j.corsci.2015.05.052.
[63] D. Li, P.P. Conway, C. Liu, Corrosion characterization of tin-lead and lead free solders in 3.5 wt.% NaCl solution, Corros. Sci. 50 (2008) 995–1004, https://doi.org/10.1016/j.corsci.2007.11.025.
[64] C.Q. Cheng, F. Yang, J. Zhao, L.H. Wang, X.G. Li, Leaching of heavy metal elements in solder alloys, Corros. Sci. 53 (2011) 1738–1747, https://doi.org/10.1016/j.corsci.2011.01.049.